

Amino Alcohol-Derived Reduced Schiff Base V^{IV}O and V^V Compounds as Catalysts for Asymmetric Sulfoxidation of Thioanisole with Hydrogen Peroxide

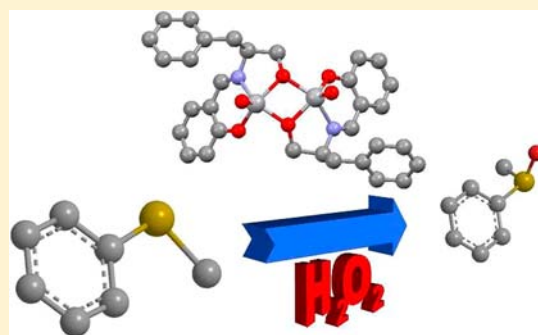
Pedro Adão,^{*,†} Maxim L. Kuznetsov,[†] Sónia Barroso,[†] Ana M. Martins,[†] F. Avecilla,[‡] and João Costa Pessoa^{*,†}

[†]Centro Química Estrutural, Instituto Superior Técnico, Universidade Técnica de Lisboa, Avenida Rovisco Pais, 1049-001 Lisboa, Portugal

[‡]Departamento de Química Fundamental, Universidade da Coruña, Campus de A Zapateira, 15071 A Coruña, Spain

Supporting Information

ABSTRACT: We report the synthesis and characterization of several amino alcohol-derived reduced Schiff base ligands (AORSB) and the corresponding V^{IV}O and V^V complexes. Some of the related Schiff base variants (amino alcohol derived Schiff base = AOSB) were also prepared and characterized. With some exceptions, all compounds are formulated as dinuclear compounds {V^{IV}O(L)}₂ in the solid state. Suitable crystals for X-ray diffraction were obtained for two of the AORSB compounds, as well as a rare X-ray structure of a chiral V^{IV}O compound, which revealed a dinuclear {V^{IV}O(AOSB)}₂ structure with a rather short V–V distance of 3.053(9) Å. Electron paramagnetic resonance (EPR), ⁵¹V NMR, and density functional theory (DFT) studies were carried out to identify the intervenient species prior to and during catalytic reactions. The quantum-chemical DFT calculations were important to determine the more stable isomers in solution, to explain the EPR data, and to assign the ⁵¹V NMR chemical shifts. The V(AORSB) and V(AOSB) complexes were tested as catalysts in the oxidation of thioanisole, with H₂O₂ as the oxidant in organic solvents. In general, high conversions of sulfoxide were obtained. The V(AOSB) systems exhibited greater activity and enantioselectivity than their V(AORSB) counterparts. Computational and spectroscopic studies were carried out to assist in the understanding of the mechanistic aspects and the reasons behind such marked differences in activity and enantioselectivity. The quantum-chemical calculations are consistent with experimental data in the assessment of the differences in catalytic activity between V(AOSB) and V(AORSB) peroxido variants because the V(AORSB) peroxido transition states correspond to ca. 22 kJ/mol higher energy activation barriers than their V(AOSB) counterparts.



INTRODUCTION

The amino alcohol-derived V^{IV}O(Schiff base) compounds are structurally simpler than the related V^{IV}O(salen), and Bolm and Bienewald in 1995¹ successfully used the *tert*-leucinol-derived V^{IV}O(Schiff base) system in asymmetric sulfoxidation. This system represented a step forward from the chiral diamine-derived V^{IV}O(salen) catalytic system reported by Fujita and co-workers² with respect to enantioselectivity and activity: the aforementioned V^{IV}O(Schiff base) system did not require low temperatures to exhibit high enantioselectivity and used cheap and environmentally benign aqueous hydrogen peroxide as the terminal oxidant instead of organic hydroperoxides; the V^{IV}O precatalyst could also be generated in situ further simplifying the application of this catalytic system. One of the major advantages of the system devised by Bolm and Bienewald was that it tapped into a much wider chiral pool, given that most commercially available chiral amino alcohols derive directly from naturally occurring compounds. The wider possibility of choice conferred a greater versatility to the amino alcohol-derived V^{IV}O(Schiff base) catalytic systems, given that the

possibilities for fine-tuning the catalyst properties were expanded despite the structural simplicity. Indeed, many authors made use of this versatility and developed important improvements on the original.

Vetter and Berkessel³ reported various *tert*-leucinol-derived V^{IV}O(Schiff base) catalysts for the asymmetric sulfoxidation of thioethers, which were based on the binaphthyl structural motif. The axial chirality exhibited by the binaphthyl moiety constituted an additional chirality element that reinforced the enantioselectivity. The intention behind this structural variation was to induce chiral amplification by introducing another element of chirality in addition to the single chiral carbon present in the amino alcohol backbone. The authors did observe a significant improvement in terms of activity and enantioselectivity as a result of chiral amplification, in particular when axial chirality was present.

Received: May 31, 2012

Published: October 23, 2012

Ahn and co-workers⁴ reported *tert*-leucinol-derived V^{IV}O- (Schiff base) catalysts based on the well-known BINOL (1,1'-bi-2-naphthol) as a means to improve activity and enantioselectivity. The authors also observed that the chirality element in the phenolate moiety by itself is not responsible for asymmetric induction. This illustrated how important it is for a given amino alcohol-derived V^{IV}O(Schiff base) that the stereogenic centers are as close as possible to the donor atoms and metal center.

Zhao and co-workers attempted to improve the amino alcohol-derived V^{IV}O(Schiff base) system using a different approach.⁵ The authors departed from the *tert*-leucinol structural motif and employed simpler and cheaper amino alcohols such as L-phenylalaninol, L-valinol, and L-isoleucinol. Cheap and commercially available salicylaldehyde was used as the aromatic aldehyde instead of the more complex substituted salicylaldehydes used in previous reports. The tandem thioether-to-sulfoxide and sulfoxide-to-sulfone oxidation processes were used to achieve enantiomeric excesses up to 99% at a cost of sulfoxide yields. Finally, the authors also noted that using preprepared V^{IV}O(Schiff base) compounds, in contrast to the in situ procedures, proved beneficial to enantioselectivity. This also minimized the ligand waste associated with the previous in situ methods.

Jackson and co-workers⁶ reported a highly selective *tert*-leucinol-derived V^{IV}O(Schiff base) system that used 3,5-diiodosalicylaldehyde as a structural precursor. High sulfoxide yields were obtained and enantiomeric excesses were better than 95% with a variety of thioether substrates. This system illustrates how minimal alterations to the original design may yield significant gains in the catalyst performance.

To demonstrate that the amino alcohol structural precursors do not need to be restricted to those directly derived from L-amino acids, Ruff and co-workers⁷ devised several in situ V^{IV}O(Schiff base) catalysts derived from D-amino sugars that gave sulfoxide yields up to 97% coupled with 60% in enantiomeric excess.

A more recent variant of Bolm's catalytic system was reported by Sun and co-workers,⁸ where the authors developed a closely related V^{IV}O catalyst based on 4-methyl-5,6,7,8-tetrahydroquinolin-8-ol. While structurally very similar, the ligand used in this system was not a Schiff base per se. In addition, the catalyst exhibited the best performance in acetone, with sulfoxide yields and enantiomeric excesses similar to those obtained initially by Bolm and Bienewald in chlorinated solvents.

Despite the various iterations of the amino alcohol-based V^{IV}O(Schiff base) catalysts, most share the same flaw inherent to Schiff base ligands: their tendency to hydrolyze in the presence of water. Moreover, Bolm's protocol and its variants rely on in situ generation of the V^{IV}O precatalyst and seem to require an excess of ligand precursor relative to the metal precursor to achieve the reported high activities and enantioselectivities. While in situ generation of the precatalyst simplifies the entire process, it may not allow adequate characterization of the precatalyst species. The excess of Schiff base ligand precursor used in Bolm's method and replicated by the successive authors who improved the design can be considered wasteful and must be inevitably separated from the final product. Nevertheless, the superior potential of amino alcohol-based V^{IV}O(Schiff base) catalysts as asymmetric sulfoxidation catalysts relative to the V^{IV}O(salen) and V^{IV}O(salan) catalysts is noteworthy.

We previously compared the use of reduced Schiff base salen complexes with their "classical" salen counterparts.⁹ V^{IV}O-(salan) compounds are much more hydrolytically stable than the corresponding V^{IV}O(salen) and showed increased activity and enantioselectivity for sulfoxidation.

Hydrolytic stability is crucial if more sustainable procedures are to be developed, particularly for large-scale synthesis. For this purpose, recyclability of the catalyst is important, and reduced Schiff base systems may be much more suitable in this respect. Thus, we used this rationale to develop amino alcohol-derived reduced Schiff base (AORSB) systems, which we expect to be much more stable under catalytic conditions. Aiming to obtain recyclable heterogenized systems, we anticipate that M(AORSB) compounds might be much more adequate than the corresponding M(AOSB) counterparts.

Moreover, because we also aim to get suitable active catalysts for asymmetric sulfoxidation, this work also intends to compare and understand the differences in activity and enantioselectivity between the V(AOSB) and V(AORSB) systems. Thus, density functional theory (DFT) calculations were also carried out to clarify the mechanisms of sulfoxidation in both systems, also trying to understand the origin of enantioselectivity.

EXPERIMENTAL SECTION

Materials and Equipment. The chiral amino alcohols L-phenylalaninol, L-valinol, and D-phenylglycinol were purchased from Fluka and Acros. Salicylaldehyde, *o*-vanillin, 3,5-di-*tert*-butylsalicylaldehyde, and 2-hydroxy-1-naphthaldehyde were purchased from Aldrich and Merck. Metal precursors V^{IV}OCl₂ (aqueous solution, 50% w/v) and V^{IV}O(acac)₂ (acac = acetylacetonate) were purchased from Carlo-Erba and Sigma-Aldrich, respectively. Thioanisole was from purchased from Acros and hydrogen peroxide (aqueous solution, 30% w/v) from Panreac and Aldrich. All chemical precursors were used as received. Solvents were purchased from Sigma-Aldrich, Carlo-Erba, Panreac, and Fisher and used as received. IR spectra were recorded with a BioRad FTS 3000 MX Fourier transform infrared spectrometer. UV-vis spectra were recorded with a Hitachi U-2000 spectrophotometer and circular dichroism (CD) spectra with a Jasco J-720 spectropolarimeter. ¹H, ¹³C, and ⁵¹V NMR spectra were obtained on Bruker Avance+ 400 and 300 MHz spectrometers. ¹H and ¹³C chemical shifts (δ) are expressed in ppm relative to Me₄Si. ⁵¹V chemical shifts are expressed in ppm relative to neat V^{IV}OCl₃. Elemental analyses were carried out at Laboratório de Análises of Instituto Superior Técnico, using a Perkin-Elmer PE 2400 Series II analyzer. Electron paramagnetic resonance (EPR) spectra were measured with a Bruker ESP 300E X-band spectrometer, normally in frozen samples at 77 K, using a perylene radical as the reference. The measured spectra (first-derivative X-band EPR) were simulated with the EPR simulation software (ROKI) developed by Rockenbauer and Korecz.¹⁰

X-ray Crystal Structure Determination of 4. Three-dimensional room temperature X-ray data were collected on a Bruker KAPPA APEX CCD diffractometer at low temperature for **4** by the ϕ - ω scan method. Reflections were measured from a hemisphere of data collected from frames, each of them covering 0.3° in ω . Of the 26449 reflections measured, all were corrected for Lorentz and polarization effects and for absorption by multiscan methods based on symmetry-equivalent and repeated reflections; 5029 independent reflections exceeded the significance level ($|I|/\sigma(I)$) > 4.0. Complex scattering factors were taken from the program package SHELXTL.¹¹⁻¹³ The structures were solved by direct methods and refined by full-matrix least squares on F^2 . The structure presents disorder in the O2 atom, which is localized in two positions around the phenyl ring. This disorder was solved, and two atomic sites have been observed and refined with anisotropic atomic displacement parameters. The site occupancy factor for O2A is 0.69364. Hydrogen atoms were left to refine freely with isotropic thermal parameters, except the hydrogen atoms of O2A, O2B, C18, C19, C20, and C24, which were included in

calculated positions and refined in the riding mode. Refinement was done with allowance for thermal anisotropy of all non-hydrogen atoms. The absolute configuration was established by refinement of the enantiomorph polarity parameter [$x = -0.02(6)$].¹³ Further details of the crystal structure determination are given in Table 1.

Table 1. Selected Crystallographic Experimental Data and Structure Refinement Parameters for 4, 8, and 13

	4	8	13·C ₄ H ₈ O
empirical formula	C ₂₄ H ₃₅ ClNO ₂	C ₁₇ H ₂₁ NO ₃	C ₃₂ H ₃₀ N ₂ O ₆ V ₂ ·C ₄ H ₈ O
mol wt	404.98	287.35	712.56
temp (K)	100(2)	150(2)	150(2)
cryst syst	orthorhombic	monoclinic	orthorhombic
space group	P2 ₁ 2 ₁ 2 ₁	P2 ₁	P2 ₁ 2 ₁ 2 ₁
a (Å)	8.688(5)	4.7570(7)	10.3880(6)
b (Å)	15.802(5)	10.2690(14)	10.5770(6)
c (Å)	16.721(5)	15.583(2)	30.3090(15)
α (deg)	90	90	90
β (deg)	90	93.403(9)	90
γ (deg)	90	90	90
V (Å ³)	2295.6(17)	759.88(18)	3330.2(3)
Z, ρ _{calc} (g/cm ³)	4, 1.172	2, 1.256	4, 1.421
μ (mm ⁻¹)	0.185	0.086	0.613
cryst size	0.36 × 0.10 × 0.09	0.40 × 0.40 × 0.05	0.10 × 0.10 × 0.04
cryst color	colorless	colorless	pink
cryst shape	prism	needle	plate
reflns collected	26449	3829	39320
unique reflns [R(int)]	5029 [0.0419]	2279 [0.0539]	5892 [0.1029]
R1 [I > 2σ(I)] ^a	0.0451	0.0542	0.0451
wR2 [I > 2σ(I)] ^b	0.1237	0.0874	0.0809
GOF on F ²	1.052	0.930	1.008
absolute structural param	-0.02(6)		-0.006(25)

^aR1 = $\sum ||F_o| - |F_c|| / \sum |F_o|$. ^bwR2 = $\{\sum [w(|F_o|^2 - |F_c|^2)]^2 / \sum [w(F_o^4)]\}^{1/2}$.

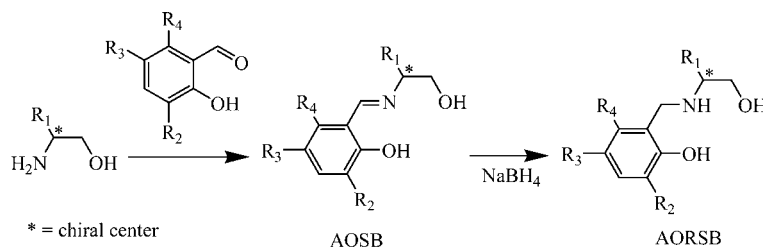
X-ray Crystal Structure Determination of 8 and 13. Single crystals suitable for X-ray diffraction crystallography were obtained as described in the Preparations section. Pertinent details for the individual compounds can be found in Table 1. Crystals were covered with polyfluoroether oil and mounted on a Nylon loop. The data were collected using graphite-monochromated Mo K α radiation ($\lambda = 0.71073$ Å) on a Bruker AXS-KAPPA APEX II diffractometer equipped with an Oxford Cryosystem open-flow nitrogen cryostat. Cell parameters were retrieved using Bruker SMART software and refined using Bruker SAINT on all observed reflections. Absorption corrections were applied using SADABS.¹¹ The structures were solved and refined using direct methods with programs SIR2004¹² or SHELXS-97.¹³ All programs are included in the package of programs WINGX, version 1.80.01,¹⁴ in SHELXL.¹⁵ All non-hydrogen atoms were refined anisotropically, and the hydrogen atoms were inserted into idealized positions and allowed to refine riding on the parent carbon atom. The molecular diagrams were drawn with ORTEP-3 for Windows¹⁶ included in the software package.

Data for compounds 4, 8, and 13 were deposited in the Cambridge Crystallographic Data Centre under deposit numbers CCDC 883783, 881019, and 881018 and can be obtained free of charge via <http://www.ccdc.cam.ac.uk/conts/retrieving.html> or from the Cambridge Crystallographic Data Centre, 12 Union Road, Cambridge CB2 1EZ, U.K., fax (+44) 1223 336 033, or e-mail deposit@ccdc.cam.ac.uk. Supporting Information associated with this article is provided.

Computational Details. The full geometry optimization of the structures was carried out at the DFT level of theory using the B3LYP¹⁷ functional with the help of the Gaussian 03¹⁸ program package. No symmetry operations were applied for any of the structures calculated. The geometry optimization was carried out using a relativistic Stuttgart pseudopotential, which describes 10 core electrons and the appropriate contracted basis set (8s7p6d1f)/[6s5p3d1f],¹⁹ for the vanadium atom and the 6-31G(d) basis set for other atoms. The Hessian matrix was calculated analytically for all optimized structures to prove the location of correct minima (no imaginary frequencies) or transition state (one imaginary frequency) and to estimate the thermodynamic parameters, with the latter being calculated at 25 °C. The nature of the transition states was investigated by analysis of the vectors associated with the imaginary frequency.

For the mechanistic part, total energies corrected for solvent effects (E_s) were estimated at the single-point calculations on the basis of gas-phase geometries at the CPCM-B3LYP//gas-B3LYP/6-31G(d) level of theory using the polarizable continuum model²⁰ in the CPCM version²¹ with CH₂Cl₂ as the solvent. The UAKS model was applied for the molecular cavity. The entropic term in solutions (S_s) was

Scheme 1. General Synthetic Method and Structural Formulas of the Amino Alcohol-Derived Compounds (Ligand Precursors) and Their Respective Designation



AOSB

5 H₂3,5-di-¹Busal(L-Pheol-im) R₁=Bn; R₂,R₃=ⁱBu; R₄=H

7 H₂naph(L-Pheol-im) R₁=Bn; R₂=H; R₃,R₄=-C₄H₄-

9 H₂mvan(L-Pheol-im) R₁=Bn; R₂=MeO; R₃,R₄=H

Bn = Benzyl

AORSB

1 H₂mvan(D-Phglyol-am) R₁=Ph; R₂=MeO; R₃,R₄=H

2 H₂sal(L-Valol-am) R₁=ⁱPr; R₂,R₃,R₄=H

3 H₂sal(L-Pheol-am) R₁=Bn; R₂,R₃,R₄=H

4 H₂3,5-di-¹Busal(L-Pheol-am) R₁=Bn; R₂,R₃=ⁱBu;

R₄=H

6 H₂naph(L-Pheol-am) R₁=Bn; R₂=H; R₃,R₄=-C₄H₄-

8 H₂mvan(L-Pheol-am) R₁=Bn; R₂=MeO; R₃,R₄=H

calculated according to the procedure described by Wertz²² and Cooper and Ziegler²³ (see the Supporting Information for details). The enthalpies and Gibbs free energies in solution (H_s and G_s) were estimated using the following equations:

$$H_s = E_s + H_g - E_g$$

$$G_s = H_s - TS_s$$

where E_s , E_g , and H_g are the total energies in solution, the gas phase and the gas-phase enthalpy, respectively.

Magnetic shielding was calculated for the equilibrium geometries using the GIAO²⁴ method at the CPCM-B3P86/6-311+G(2d,p)//gas-B3P86/6-31G(d) level including the solvent effects with CH_2Cl_2 as the solvent. The geometry optimization was carried out at the B3P86 level because this functional reproduces better ^{51}V NMR chemical shifts of vanadium complexes with Schiff bases in comparison with the B3LYP functional.²⁵ ^{51}V chemical shifts ($\delta^{\text{V}}_{\text{calc}}$) were estimated relative to VOCl_3 (σ of -2914 calculated at the same level of theory).

The ^{51}V hyperfine coupling constants in the V^{IV} complexes were estimated at the single-point calculations using the BHandHLYP functional and 6-311+G* basis set for all atoms on the basis of the equilibrium geometry obtained at the B3LYP/6-31G(d)(V-ECP) level of theory. The anisotropic ^{51}V hyperfine coupling constants A_x , A_y , and A_z were estimated as the sum of the isotropic Fermi contact term and corresponding dipolar hyperfine interaction term.²⁶

Preparations. Synthesis of Ligand Precursors. The ligands were synthesized by adapting previously published procedures.⁹ Single crystals adequate for X-ray diffraction studies were obtained for some of the ligands. The structural formulas of the ligand precursor compounds are shown in Scheme 1.

$H_3\text{mvan}(D\text{-Phglyol-am})\text{Cl}$, 1. *D*-Phenylglycinol (1.5 g, 10.9 mmol) was condensed with 3-methoxysalicylaldehyde (1.67 g, 11.0 mmol) in 25 mL of methanol. Solid NaBH_4 was added to the solution until it became colorless. The pH was then adjusted to approximately 2 with an aqueous 4 M HCl solution. The solvent was evaporated and the white residue extracted with isopropyl alcohol, with the inorganic solids being separated by filtration. By evaporation of the solvent, a white hygroscopic solid was obtained, which was then washed with diethyl ether. The free compound is a viscous oil, and conversion to the respective hydrochloride salt was required. A hygroscopic off-white solid was obtained. Yield: 2.9 g, 85%. ^1H NMR (400 MHz, $\text{DMSO-}d_6$, ppm): δ 3.78 [3H, s, CH_3OAr], 4.24 [1H, s, $\text{ArCH}(\text{CH}_2\text{OH})$], 3.93 [2H, m, $-\text{CH}_2\text{OH}$], 3.93 [2H, s, $\text{ArCH}_2\text{N}^+\text{H}_2$], 6.77, 6.98, 7.41 [8H, m, aromatic]. $^{13}\text{C}\{^1\text{H}\}$ NMR (100 MHz, $\text{DMSO-}d_6$, ppm): δ 43 [1C, $\text{ArCH}_2\text{N}^+\text{H}_2$], 56 [1C, CH_3OAr], 62 [1C, $-\text{CH}_2\text{OH}$], 63 [1C, $\text{ArCH}(\text{CH}_2\text{OH})$], 112, 118, 119, 123, 127.7, 128.4, 128.6, 128.8, 128.9, 133.6, 145, 147 [12C, aromatic]. IR (cm^{-1}): 3369 ($\nu_{\text{N-H}}$), 1493 ($\nu_{\text{C=C}}$), 1223 ($\nu_{\text{C-O}}$). Elem anal. Calcd for $\text{C}_{16}\text{H}_{20}\text{NO}_3\text{Cl}\cdot 2\text{H}_2\text{O}$: C, 55.57; H, 6.99; N, 4.05. Found: C, 55.3; H, 6.8; N, 4.1.

$H_3\text{sal}(L\text{-Valol-am})\text{Cl}$, 2. The procedure was similar to that used for the synthesis of 1. Reagents: *L*-valinol (1.00 g, 9.7 mmol); salicylaldehyde (1.19 g, 9.7 mmol). Ethanol was used instead of isopropyl alcohol during the hydrochloride salt extraction steps. The compound was obtained as a white hygroscopic solid. Yield: 1.89 g, 80%. ^1H NMR (300 MHz, $\text{DMSO-}d_6$, ppm): δ 0.95 [6H, t, $^3J_{\text{HH}} = 7$ Hz, $(\text{CH}_3)_2\text{CH}-$], 2.15 [1H, m, $(\text{CH}_3)_2\text{CH}-$], 2.84 [1H, m, $\text{PrCH}-$], 3.65, 3.73 [2H, m, $-\text{CH}_2\text{OH}$], 4.18 [2H, s, $\text{ArCH}_2\text{N}^+\text{H}_2$], 6.81, 7.01, 7.21, 7.49 [4H, m, aromatic]. $^{13}\text{C}\{^1\text{H}\}$ NMR (75 MHz, $\text{DMSO-}d_6$, ppm): δ 17.59, 19.31 [2C, $(\text{CH}_3)_2\text{CH}-$], 26.15 [1C, $(\text{CH}_3)_2\text{CH}-$], 43.95 [1C, $\text{ArCH}_2\text{N}^+\text{H}_2$], 57.29 [1C, $-\text{CH}_2\text{OH}$], 63.45 [1C, $\text{PrCH}-$], 115.55, 118.04, 119.04, 130.27, 131.82, 156.36 [6C, aromatic]. IR (cm^{-1}): 3143 ($\nu_{\text{N-H}}$), 1506 ($\nu_{\text{C=C}}$), 1266 ($\nu_{\text{C-O}}$). Elem anal. Calcd for $\text{C}_{12}\text{H}_{20}\text{NO}_2\text{Cl}\cdot 0.5\text{C}_2\text{H}_5\text{OH}$: C, 58.09; H, 8.62; N, 5.21. Found: C, 58.2; H, 8.9; N, 5.5.

$H_2\text{sal}(L\text{-Pheol-am})$, 3. The procedure was similar to that used for the synthesis of 1. Reagents: *L*-phenylalaninol (1.00 g, 6.6 mmol); salicylaldehyde (0.81 g, 6.6 mmol). It was found that neutralization of the hydrochloride salt with NaHCO_3 in an aqueous medium induced precipitation of a flaky white solid. Alternatively, 150 mL of water may be added to the reaction mixture after the reduction step to induce

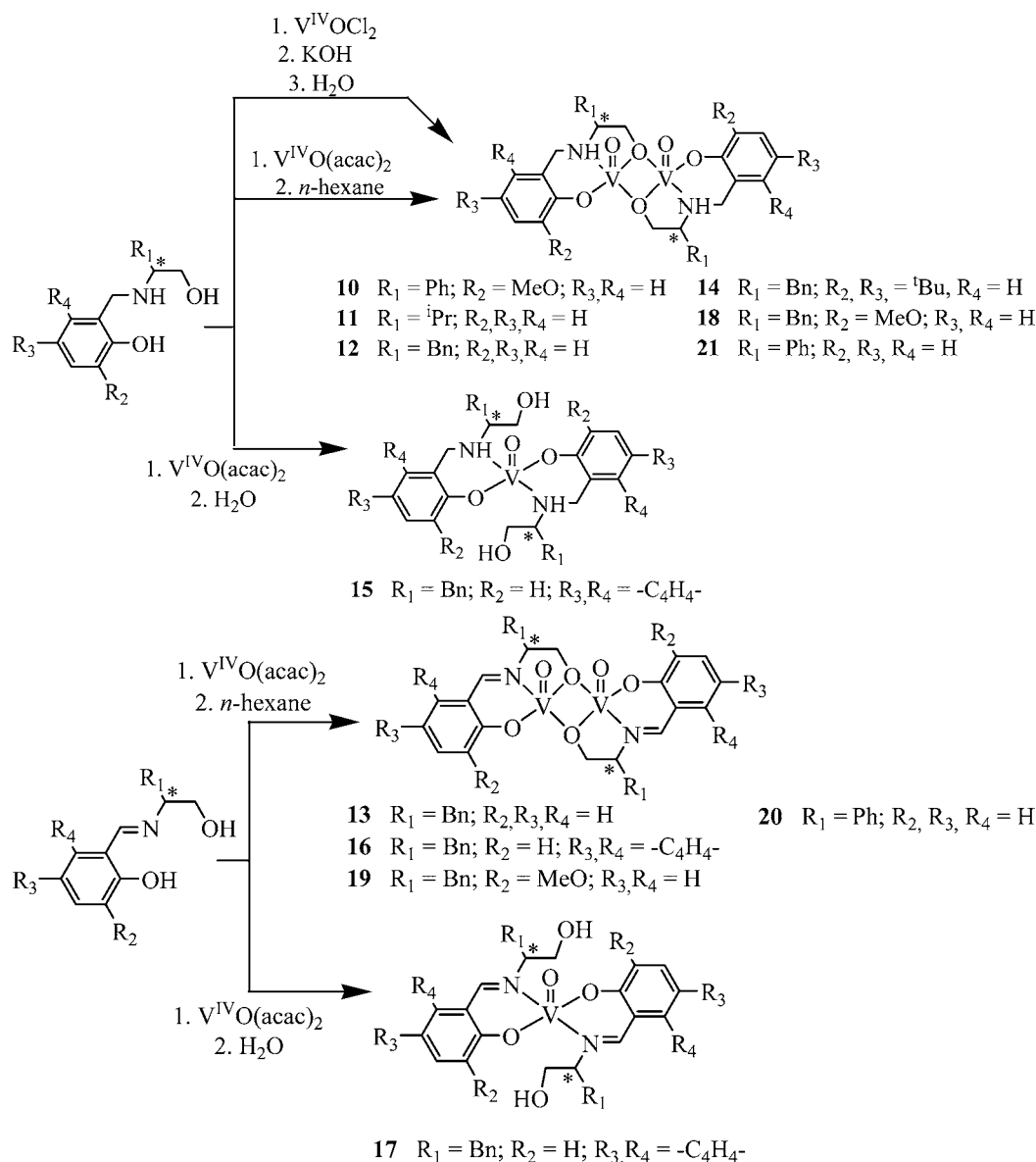
precipitation. The free base could be obtained as a white solid. Yield: 1.10 g, 65%. ^1H NMR (300 MHz, $\text{DMSO-}d_6$, ppm): δ 2.73 [2H, m, $\text{ArCH}_2\text{CH}-$], 2.73 [1H, m, $\text{ArCH}_2\text{CH}-$], 3.30, 3.41 [2H, m, $-\text{CH}_2\text{OH}$], 3.85 [2H, s, $\text{ArCH}_2\text{N}^+\text{H}_2$], 6.69, 7.05, 7.19, 7.27 [9H, m, aromatic]. $^{13}\text{C}\{^1\text{H}\}$ NMR (75 MHz, $\text{DMSO-}d_6$, ppm): δ 37.613 [1C, $\text{ArCH}_2\text{CH}-$], 48.06 [1C, $\text{ArCH}_2\text{N}^+\text{H}_2$], 60.21 [1C, $\text{ArCH}_2\text{CH}-$], 61.89 [1C, $-\text{CH}_2\text{OH}$], 155.18, 118.79, 125.17, 126.27, 128.19, 128.57, 128.92, 129.60, 139.83, 157.63 [12C, aromatic]. IR (cm^{-1}): 3318 ($\nu_{\text{N-H}}$), 1458 ($\nu_{\text{C=C}}$), 1241 ($\nu_{\text{C-O}}$). Elem anal. Calcd for $\text{C}_{16}\text{H}_{19}\text{NO}_2$: C, 74.67; H, 7.44; N, 5.44. Found: C, 74.2; H, 7.8; N, 5.4.

$H_{3,5}\text{-di-}t\text{Busal}(L\text{-Pheol-am})\text{Cl}$, 4. The procedure was similar to that used for the synthesis of 1. Reagents: *L*-phenylalaninol (1.00 g, 6.6 mmol); 3,5-di-*tert*-butylsalicylaldehyde (1.55 g, 6.6 mmol). The compound was obtained as an off-white solid. Yield: 2.15 g, 80%. ^1H NMR (300 MHz, $\text{DMSO-}d_6$, ppm): δ 1.27, 1.43 [18H, s, $\text{ArC}(\text{CH}_3)_3$], 2.91, 3.20 [2H, t, $^3J_{\text{HH}} = 12.0$ Hz, $\text{ArCH}_2\text{CH}-$], 3.37 [1H, m, $\text{ArCH}_2\text{CH}-$], 3.47, 3.68 [2H, d, $^2J_{\text{HH}} = 11.8$ Hz, $-\text{CH}_2\text{OH}$], 4.29 [2H, m, $\text{ArCH}_2\text{N}^+\text{H}_2$], 7.29 [7H, m, aromatic]. $^{13}\text{C}\{^1\text{H}\}$ NMR (75 MHz, $\text{DMSO-}d_6$, ppm): δ 30.07, 32.12 [6C, $\text{ArC}(\text{CH}_3)_3$], 34.04 [1C, $\text{ArCH}_2\text{CH}-$], 34.68, 35.75 [2C, $\text{ArC}(\text{CH}_3)_3$], 45.00 [1C, $\text{ArCH}_2\text{N}^+\text{H}_2$], 58.42 [1C, $-\text{CH}_2\text{OH}$], 61.15 [1C, $\text{ArCH}_2\text{CH}-$], 122.52, 124.96, 127.61, 129.40, 130.10, 137.79, 140.02, 143.16, 152.61 [12C, aromatic]. IR (cm^{-1}): 3300 ($\nu_{\text{N-H}}$), 1466 ($\nu_{\text{C=C}}$), 1250 ($\nu_{\text{C-O}}$). Elem anal. Calcd for $\text{C}_{24}\text{H}_{36}\text{NO}_2\text{Cl}$: C, 71.00; H, 8.94; N, 3.45. Found: C, 71.3; H, 9.5; N, 3.5. Crystals suitable for single-crystal X-ray diffraction were grown from isopropyl alcohol solutions. A total of 0.1 g of 4 was dissolved in ca. 10 mL of isopropyl alcohol, and the resulting solution was filtered and transferred to a clean lint-free 20 mL glass flask. Colorless crystals were obtained by slow evaporation of the solvent after 4 weeks.

$H_{2,3}\text{-di-}t\text{Busal}(L\text{-Pheol-im})$, 5. The procedure was similar to that used for the synthesis of 1 but without the reduction step. The solvent was evaporated completely, and the yellow residue was washed with small portions of a 1:1 ethanol/water mixture and diethyl ether. Reagents: *L*-phenylalaninol (0.53 g, 3.5 mmol); 3,5-di-*tert*-butylsalicylaldehyde (0.82 g, 3.5 mmol). The compound was obtained as a bright-yellow solid. Yield: 1.09 g, 85%. ^1H NMR (400 MHz, CDCl_3 , ppm): δ 1.43, 1.60 [18H, s, $\text{ArC}(\text{CH}_3)_3$], 3.08 [2H, m, $\text{ArCH}_2\text{CH}-$], 3.67 [1H, m, $\text{ArCH}_2\text{CH}-$], 3.92 [2H, m, $-\text{CH}_2\text{OH}$], 7.15 [1H, d, $^4J_{\text{HH}} = 2.4$ Hz, aromatic], 7.33, 7.41 [5H, m, aromatic], 7.53 [1H, d, $^4J_{\text{HH}} = 2.4$ Hz, aromatic], 8.33 [2H, m, $\text{ArCH}=\text{N}$]. $^{13}\text{C}\{^1\text{H}\}$ NMR (75 MHz, $\text{DMSO-}d_6$, ppm): δ 29.74, 31.45 [6C, $\text{ArC}(\text{CH}_3)_3$], 34.18, 35.25 [2C, $\text{ArC}(\text{CH}_3)_3$], 39.48, [1C, $\text{ArCH}_2\text{CH}-$], 66.30 [1C, $-\text{CH}_2\text{OH}$], 73.69 [1C, $\text{ArCH}_2\text{CH}-$], 117.52, 126.32, 126.56, 127.34, 128.31, 129.58, 136.79, 138.16, 140.32, 158.16 [12C, aromatic], 167.36 [1C, $\text{ArCH}=\text{N}$]. IR (cm^{-1}): 1626 ($\nu_{\text{C=N}}$), 1250 ($\nu_{\text{C-O}}$). Elem anal. Calcd for $\text{C}_{24}\text{H}_{33}\text{NO}_2\cdot 0.2\text{C}_2\text{H}_5\text{OH}$: C, 77.79; H, 9.15; N, 3.72. Found: C, 77.7; H, 9.4; N, 4.0.

$H_2\text{naph}(L\text{-Pheol-am})$, 6. The procedure was similar to that used for the synthesis of 1. Ethanol was used as the reaction solvent instead of methanol. Reagents: *L*-phenylalaninol (0.32 g, 2.1 mmol); 2-hydroxy-1-naphthaldehyde (0.36 g, 2.1 mmol). The hydrochloride salt was obtained as an off-white solid. Alternatively, the free base can be obtained by the addition of ca. 100 mL of saturated solution of NaHCO_3 in water to the reaction mixture after the reduction step. Yield (free base): 0.5 g, 78%. ^1H NMR (300 MHz, CD_3OD , ppm): δ 2.82, 2.90 [2H, m, $\text{ArCH}_2\text{CH}-$], 2.99 [1H, m, $\text{ArCH}_2\text{CH}-$], 3.52, 3.61 [2H, m, $-\text{CH}_2\text{OH}$], 4.37 [2H, dd, $^2J_{\text{HH}} = 13.9$ and 31.0 Hz, ArCH_2NH], 7.04, 7.21, 7.39, 7.71 [11H, m, aromatic]. $^{13}\text{C}\{^1\text{H}\}$ NMR (75 MHz, CD_3OD , ppm): δ 36.27 [1C, $\text{ArCH}_2\text{CH}-$], 43.21 [1C, ArCH_2NH], 61.98 [1C, $\text{ArCH}_2\text{CH}-$], 67.38 [1C, $-\text{CH}_2\text{OH}$], 115.40, 121.79, 121.88, 124.11, 127.65, 128.10, 128.92, 129.65, 129.96, 130.11, 130.25, 130.29, 130.96, 133.33, 138.42, 157.29 [16C, aromatic]. IR (cm^{-1}): 3318 ($\nu_{\text{N-H}}$), 1458 ($\nu_{\text{C=C}}$), 1241 ($\nu_{\text{C-O}}$). Elem anal. Calcd for $\text{C}_{20}\text{H}_{22}\text{NO}_2\text{Cl}$: C, 69.86; H, 6.45; N, 4.07. Found: C, 70.2; H, 6.3; N, 3.8. Elem anal. Calcd for $\text{C}_{20}\text{H}_{21}\text{NO}_2\cdot 0.5\text{C}_2\text{H}_5\text{OH}$ (free base): C, 76.34; H, 7.32; N, 4.24. Found: C, 76.7; H, 6.9; N, 4.6.

$H_2\text{naph}(L\text{-Pheol-im})$, 7. The procedure was similar to that used for the synthesis of 5. Reagents: *L*-phenylalaninol (0.9 g, 6.0 mmol); 2-

Scheme 2. Structural Formulas of the Amino Alcohol-Derived V^{IV}O Complexes, with Compounds 20 and 21 Being Theoretical Models

hydroxy-1-naphthaldehyde (1.0 g, 6.0 mmol). The compound was obtained as a bright-yellow solid. Yield: 1.7 g, 93%. ¹H NMR (300 MHz, CD₃OD, ppm): δ 2.96, 3.12 [2H, m, ArCH₂CH-], 3.74, 3.86 [2H, m, -CH₂OH], 3.91 [1H, m, ArCH₂CH-], 6.76, 7.17, 7.26, 7.35, 7.56, 7.72 [11H, m, aromatic], 8.63 [1H, s, -N=CH-]. ¹³C{¹H} NMR (75 MHz, CD₃OD, ppm): δ 39.42 [1C, ArCH₂CH-], 64.73 [1C, -CH₂OH], 66.61 [1C, ArCH₂CH-], 119.22, 123.77, 126.15, 127.92, 129.30, 129.70, 130.18, 130.78, 139.66, 155.40 [16C, aromatic], 179.54 [1C, ArCH=N]. IR (cm⁻¹): 1626 (ν_{C=N}), 1250 (ν_{C-O}). Elem. anal. Calcd for C₂₀H₁₉NO₂: C, 78.66; H, 6.27; N, 4.59. Found: C, 78.4; H, 6.3; N, 4.3.

*H*₂*mvan*(*L*-*Pheol-am*), **8**. The procedure was similar to that used for the synthesis of **3**. Reagents: *L*-phenylalaninol (0.8 g, 5.3 mmol); *o*-vanillin (0.80 g, 5.3 mmol). The compound was obtained as the free base. Yield: 1.4 g, 92%. ¹H NMR (300 MHz, CD₃OD, ppm): δ 2.72, 2.82 [2H, m, ArCH₂CH-], 2.86 [1H, m, ArCH₂CH-], 3.43, 3.54 [2H, m, -CH₂OH], 3.82 [3H, s, CH₃OAr], 6.69, 6.74, 6.85, 7.16, 7.24 [8H, m, aromatic]. ¹³C{¹H} NMR (75 MHz, CD₃OD, ppm): δ 38.06 [1C, ArCH₂CH-], 48.55 [1C, ArCH₂NH], 56.66 [1C, CH₃OAr], 60.66 [1C, ArCH₂CH-], 63.69 [1C, -CH₂OH], 112.02, 119.92, 122.79, 125.74, 127.32, 129.48, 130.26, 140.02, 147.05, 149.00 [12C,

aromatic]. IR (cm⁻¹): 3291 (ν_{N-H}), 1626 (ν_{C=N}), 1276 (ν_{C-O}). Elem. anal. Calcd for C₁₇H₂₁NO₃: C, 71.06; H, 7.37; N, 4.94. Found: C, 70.7; H, 7.4; N, 5.0. Crystals suitable for single-crystal X-ray diffraction were grown from isopropyl alcohol solutions. A total of 0.1 g of **8** was dissolved in ca. 10 mL of isopropyl alcohol, and the resulting solution was filtered and transferred to a clean lint-free 20 mL glass flask. Colorless crystals were obtained by slow evaporation of the solvent after 4 weeks.

*H*₂*mvan*(*L*-*Pheol-im*), **9**. The procedure was similar to that used for the synthesis of **5**. Reagents: *L*-phenylalaninol (1.2 g, 7.7 mmol); *o*-vanillin (1.2 g, 7.7 mmol). The compound was obtained as a bright-yellow solid. Yield: 2.1g, 96%. ¹H NMR (300 MHz, CD₃OD, ppm): δ 2.85 [1H, dd, ²J_{HH} = 8.5 and 13.5 Hz, ArCH₂CH-], 3.05 [1H, dd, ²J_{HH} = 4.4 and 13.5 Hz, ArCH₂CH-], 3.66 [1H, m, ArCH₂CH-], 3.66, 3.78 [2H, m, -CH₂OH], 3.83 [3H, s, CH₃OAr], 6.64 [1H, t, ³J_{HH} = 7.9 Hz, aromatic], 6.75 [1H, t, ³J_{HH} = 7.9 Hz, ⁴J_{HH} = 1.4 Hz, aromatic], 6.63 [1H, t, ³J_{HH} = 7.8 Hz, ⁴J_{HH} = 1.3 Hz, aromatic], 7.17 [5H, m, aromatic], 8.05 [1H, s, -N=CH-]. ¹³C{¹H} NMR (75 MHz, CD₃OD, ppm): δ 40.02 [1C, ArCH₂CH-], 56.33 [1C, CH₃OAr], 65.47 [1C, -CH₂OH], 72.54 [1C, ArCH₂CH-], 115.54, 117.77, 118.60, 124.77, 127.50, 129.46, 130.58, 139.18, 150.09,

156.42 [$\nu_{C=N}$], 167.07 [ν_{C-O}], IR (cm^{-1}): 1641 ($\nu_{C=N}$), 1248 (ν_{C-O}). Elem anal. Calcd for $C_{17}H_{19}NO_3$: C, 71.56; H, 6.71; N, 4.91. Found: C, 71.3; H, 6.8; N, 5.0.

Synthesis of $V^{IV}O$ Complexes. The compounds were synthesized by adapting previously published procedures that employ $V^{IV}OCl_2$,^{9a,b} but alternative preparation routes using $V^{IV}O(acac)_2$ were also used. The obtained compounds are soluble in diethyl ether. As such, *n*-hexane was used instead to remove organic impurities. The proposed structural formulas of the $V^{IV}O$ complexes are shown in Scheme 2.

$\{V^{IV}O[mvan(D\text{-}Phglyol\text{-}am)]\}_2$, 10. $V^{IV}OCl_2$ (0.14 g, 0.8 mmol) was added to a methanolic (25 mL) solution of 1 (0.25 g, 0.8 mmol) under an inert (N_2) atmosphere. The pH was adjusted to ca. 7–8 with a 2 M aqueous solution of KOH. The addition of water (75 mL) induced the complete precipitation of the $V^{IV}O$ compound. The precipitate was filtered and washed with water, a minimal amount of methanol, and *n*-hexane. The solid was then dried under vacuum. The compound was obtained as a brown solid. Yield: 0.11 g, 40%. EPR (DMF, 77 K): $A_z^1 = 149.0 \times 10^{-4} \text{ cm}^{-1}$; $A_z^2 = 165.0 \times 10^{-4} \text{ cm}^{-1}$; $g_z^1 = 1.962$. IR (cm^{-1}): 1276 (ν_{C-O}), 856 ($\nu_{V=O}$). Elem anal. Calcd for $C_{32}H_{34}N_2O_8V_2 \cdot 3.5H_2O$: C, 54.32; H, 5.84; N, 3.96. Found: C, 54.1; H, 5.4; N, 3.9.

$\{V^{IV}O[sal(L\text{-}Valol\text{-}am)]\}_2$, 11. The procedure was similar to that used for the synthesis of 10. Reagents: $V^{IV}OCl_2$ (0.4 g, 2.0 mmol); 2 (2.5 g, 2.0 mmol). The compound was obtained as a light-brown solid. Yield: 0.14 g, 26%. EPR (DMF, 77 K): $A_z = 168.5 \times 10^{-4} \text{ cm}^{-1}$; $g_z = 1.948$. IR (cm^{-1}): 3185 (ν_{N-H}), 1261 (ν_{C-O}), 974, 930 ($\nu_{V=O}$). Elem anal. Calcd for $C_{24}H_{34}N_2O_8V_2 \cdot 3.5CH_3OH$: C, 50.01; H, 7.33; N, 4.24. Found: C, 49.8; H, 7.5; N, 4.7.

$\{V^{IV}O[sal(L\text{-}Pheol\text{-}am)]\}_2$, 12. The procedure was also similar to that used for the synthesis of 10. Reagents: $V^{IV}OCl_2$ (0.34 g, 2.0 mmol); 3 (0.5 g, 2.0 mmol). The compound was obtained as a violet solid. Yield: 0.25 g, 39%. EPR (DMF, 77 K): $A_z = 167.8 \times 10^{-4} \text{ cm}^{-1}$; $g_z = 1.948$. IR (cm^{-1}): 3255 (ν_{N-H}), 1269 (ν_{C-O}), 978, 936 ($\nu_{V=O}$). Elem anal. Calcd for $C_{32}H_{34}N_2O_8V_2 \cdot 2H_2O$: C, 56.48; H, 5.63; N, 4.12. Found: C, 56.7; H, 5.3; N, 4.2.

This compound was also prepared using $V^{IV}O(acac)_2$ as the metal precursor. 3 (0.42 g, 1.6 mmol) was dissolved in THF (25 mL) under an inert (N_2) atmosphere. $V^{IV}O(acac)_2$ (0.42 g, 1.6 mmol) was then added to the THF solution of 3, and the mixture was left stirring for 45 min. Then *n*-hexane (100 mL) was added to induce precipitation of the desired complex as a light-violet solid. The solid was filtered and washed with THF and *n*-hexane. Yield: 0.4 g, 75%. IR (cm^{-1}): 3250 (ν_{N-H}), 1271 (ν_{C-O}), 962 ($\nu_{V=O}$). Elem anal. Calcd for $C_{32}H_{34}N_2O_8V_2 \cdot THF$: C, 60.93; H, 6.39; N, 3.55. Found: C, 61.3; H, 6.0; N, 4.0.

$\{V^{IV}O[sal(L\text{-}Pheol\text{-}im)]\}_2$, 13. Given that the respective Schiff base ligand precursor compound was difficult to isolate in a pure form, the procedure used in this case resorted to the in situ formation of the Schiff base ligand precursor (*L*-phenylalaninol, 0.50 g, 3.3 mmol; salicylaldehyde, 0.40 g, 3.3 mmol) in THF (25 mL) and the subsequent addition of $V^{IV}O(acac)_2$ (0.87 g, 3.3 mmol) to the reaction mixture, under an inert (N_2) atmosphere. After stirring for 45 min, *n*-hexane (100 mL) was added to the mixture to induce precipitation of the desired complex. The resulting violet solid was recovered by filtration and washed with *n*-hexane. Yield: 0.62 g, 58%. IR (cm^{-1}): 1650 ($\nu_{N=C}$), 1297 (ν_{C-O}), 992 ($\nu_{V=O}$). Elem anal. Calcd for $C_{32}H_{30}N_2O_8V_2$: C, 60.01; H, 4.72; N, 4.37. Found: C, 59.6; H, 4.7; N, 4.4. Crystals suitable for single-crystal X-ray diffraction were grown from isopropyl alcohol solutions. A total of 0.1 g of 13 was dissolved in ca. 10 mL of a 1:1 THF/diethyl ether mixture, and the resulting solution was filtered and transferred to a clean lint-free 20 mL glass flask. The flask was sealed and put in a freezer for 2 weeks. A crop of green needles, red needles, and pink plates was obtained, of which only the pink plates were suitable for single-crystal X-ray diffraction

$\{V^{IV}O[3,5\text{-}dibusal(L\text{-}Pheol\text{-}am)]\}_2$, 14. The procedure was similar to that used for the synthesis of 10. Reagents: $V^{IV}OCl_2$ (0.2 g, 1.2 mmol); 4 (0.50 g, 1.2 mmol). The compound was obtained as a dark-brown solid. Yield: 0.2 g, 38%. EPR (DMF, 77 K): $A_z = 168.5 \times 10^{-4} \text{ cm}^{-1}$; $g_z = 1.948$. IR (cm^{-1}): 3262 (ν_{N-H}), 1239 (ν_{C-O}), 983 ($\nu_{V=O}$).

Elem anal. Calcd for $C_{48}H_{66}N_2O_6V_2 \cdot 0.5H_2O$: C, 65.67; H, 7.69; N, 3.19. Found: C, 65.8; H, 7.9; N, 3.2.

$\{V^{IV}O[naph(L\text{-}Pheol\text{-}am)]\}_2$, 15. The procedure was similar to that used for the alternative synthesis of 12 using $V^{IV}O(acac)_2$. Reagents: $V^{IV}O(acac)_2$ (0.42 g, 1.6 mmol); 6 (0.50 g, 1.6 mmol). Water was used instead of *n*-hexane to induce precipitation of the desired complex. The compound was obtained as a gray solid. Yield: 0.4 g, 74%. EPR (EtOH, 77 K): $A_z = 163.9 \times 10^{-4} \text{ cm}^{-1}$; $g_z = 1.951$. IR (cm^{-1}): 1252 (ν_{C-O}), 866 ($\nu_{V=O}$). Elem anal. Calcd for $C_{40}H_{40}N_2O_5V_2 \cdot 2.5H_2O$: C, 66.29; H, 6.26; N, 3.87. Found: C, 66.5; H, 6.2; N, 3.6.

$\{V^{IV}O[naph(L\text{-}Pheol\text{-}im)]\}_2$, 16. The procedure was similar to that used for the alternative synthesis of 12 using $V^{IV}O(acac)_2$. Reagents: $V^{IV}O(acac)_2$ (0.26 g, 1 mmol); 7 (0.30 g, 1 mmol). The compound was obtained as a yellow-green solid. Yield: 0.35 g, 94%. EPR (DMF, 77 K): $A_z = 168.2 \times 10^{-4} \text{ cm}^{-1}$; $g_z = 1.948$. IR (cm^{-1}): 1675 ($\nu_{N=C}$), 1340 (ν_{C-O}), 993 ($\nu_{V=O}$). Elem anal. Calcd for $C_{40}H_{34}N_2O_6V_2 \cdot 0.5H_2O$: C, 64.09; H, 4.71; N, 3.74. Found: C, 63.8; H, 4.9; N, 3.3.

The same compound was obtained when water was used instead of *n*-hexane to induce precipitation. Yield: 0.28 g, 75%. Elem anal. Calcd for $C_{40}H_{34}N_2O_6V_2$: C, 64.87; H, 4.63; N, 3.78. Found: C, 64.7; H, 4.7; N, 3.7.

$\{V^{IV}O[naph(L\text{-}Pheol\text{-}im)]\}_2$, 17. The procedure was similar to that used for the synthesis of 15 using $V^{IV}O(acac)_2$. Reagents: $V^{IV}O(acac)_2$ (0.42 g, 1.6 mmol); 7 (0.50 g, 1.2 mmol). The compound was obtained as an olive-green solid. Yield: 0.45 g, 83%. IR (cm^{-1}): 3288 (ν_{O-H}), 1620 ($\nu_{N=C}$), 1357 (ν_{C-O}), 993 ($\nu_{V=O}$). Elem anal. Calcd for $C_{40}H_{36}N_2O_5V_2 \cdot H_2O$: C, 69.26; H, 5.52; N, 4.04. Found: C, 69.5; H, 5.3; N, 4.0.

$\{V^{IV}O[mvan(L\text{-}Pheol\text{-}am)]\}_2$, 18. The procedure was similar to that used for the alternative synthesis of 12 using $V^{IV}O(acac)_2$. Reagents: $V^{IV}O(acac)_2$ (0.50 g, 1.8 mmol); 8 (0.50 g, 1.7 mmol). The compound was obtained as a violet solid. Yield: 0.59 g, 98%. EPR (DMF, 77 K): $A_z = 166.3 \times 10^{-4} \text{ cm}^{-1}$; $g_z = 1.947$. IR (cm^{-1}): 1248 (ν_{C-O}), 958 ($\nu_{V=O}$). Elem anal. Calcd for $C_{34}H_{38}N_2O_8V_2 \cdot 0.5THF$: C, 58.39; H, 5.72; N, 3.78. Found: C, 58.7; H, 5.8; N, 3.9.

$\{V^{IV}O[mvan(L\text{-}Pheol\text{-}im)]\}_2$, 19. The procedure was similar to that used for the alternative synthesis of 12 using $V^{IV}O(acac)_2$. Reagents: $V^{IV}O(acac)_2$ (0.6 g, 2.3 mmol); 9 (0.64 g, 2.2 mmol). The compound was obtained as a light-brown solid. Yield: 0.61 g, 78%. EPR (DMF, 77 K): $A_z = 169.9 \times 10^{-4} \text{ cm}^{-1}$; $g_z = 1.947$. IR (cm^{-1}): 1626 ($\nu_{N=C}$), 1250 (ν_{C-O}), 989 ($\nu_{V=O}$). Elem anal. Calcd for $C_{34}H_{34}N_2O_8V_2 \cdot 0.5H_2O$: C, 57.55; H, 4.97; N, 3.95. Found: C, 57.5; H, 5.0; N, 4.0.

Procedure for Sulfoxidation. The catalytic experiments were carried out at atmospheric pressure at set constant temperatures in a glass batch reactor, equipped with a magnetic stirrer, a thermometer, and a condenser. In a typical run, the solid catalyst and thioanisole (1.0 mmol) were dissolved in the appropriate solvent (4 mL). Then the oxidant (1.2–1.5 mmol) and hydrogen peroxide (30 w/w aqueous solution) were added to the stirring mixture. Control experiments were also carried out in the absence of catalyst.

Analysis of products of sulfoxidation was done by high-performance liquid chromatography (HPLC; Jasco system with an Intelligent 880-PU HPLC pump, a two-line degasser 880-51, an Intelligent 870-UV UV-vis detector, and a Rheodyne 725i injector (5 μL), using a Daicel Chiralpak IA column and a Borwin software). The eluent used was hexane/ethyl acetate (60:40) with a flow rate of 1 mL/min. The calibration curves for each reagent and product, namely, sulfoxide and sulfone, were determined using similar HPLC procedures and these calibrations used for quantitative analyses. Diphenylsulfone was used as an internal standard.⁹

RESULTS AND DISCUSSION

Synthesis and Characterization of the Ligand Precursors. The reduced Schiff base ligand precursors were prepared in a two-step, one-pot reaction: condensation of the chiral amino alcohol with 1 equiv of 2-hydroxybenzaldehyde

followed by reduction with solid NaBH_4 . For the Schiff base compounds, the reduction step was not done.

Crystals of **4** and **8** suitable for single-crystal X-ray diffraction were grown from isopropyl alcohol solutions at room temperature. The molecular structures of **4** and **8** are depicted in Figure 1, and relevant distances and angles are presented in

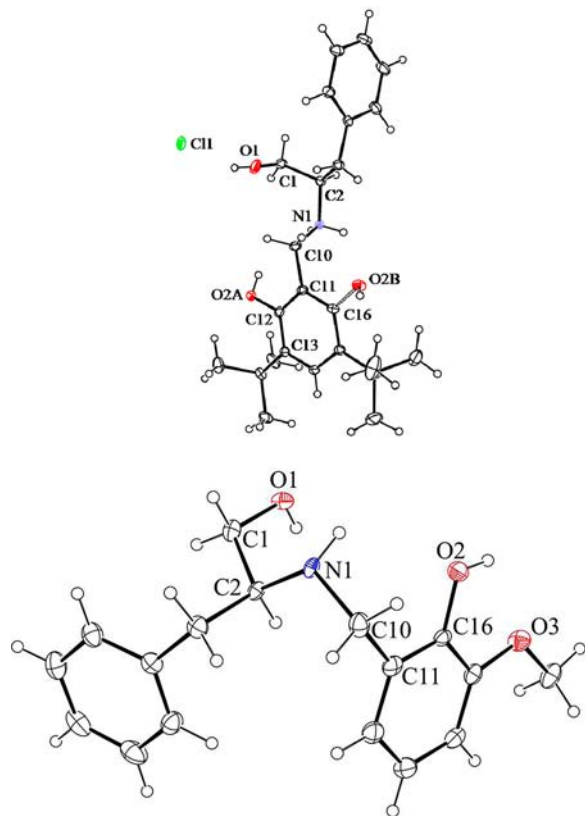


Figure 1. ORTEP representations of **4** (using 30% probability ellipsoids) and **8** (using 30% probability ellipsoids).

Table 2. While **8** is a neutral compound, crystals of **4** contain the protonated ligand and one Cl^- anion in the asymmetric unit. The C–N bond distances are 1.511(3) Å (for **4**) and 1.500(5) Å (for **8**), lengths typical of C–N single bonds. The Cl^- anion is involved in four strong hydrogen bonds responsible of the three-dimensional crystal packing structure (see Figures SI-10 and SI-11 in the Supporting Information), in which it is observed that three molecules of **4** interact with the same Cl^- anion.

Synthesis and Characterization of the $\text{V}^{\text{IV}}\text{O}$ and V^{V} Complexes. Globally, the elemental analyses and spectroscopic data (see below) are consistent with formulation of most of the vanadium compounds isolated as dinuclear $[\text{V}^{\text{IV}}\text{OL}]_2$ complexes. Compounds **15** and **17** are formulated as $\text{V}^{\text{IV}}\text{O}(\text{L})_2$ compounds.

We found that, similar to the $\text{V}^{\text{IV}}\text{O}$ -salen and $\text{V}^{\text{IV}}\text{O}$ -salan compounds studied earlier by some of us, coloration in the solid state also depends on whether the compound has $\text{V}=\text{O}\cdots\text{V}=\text{O}$ interactions and/or C=N bonds. Schiff base compounds lacking $\text{V}=\text{O}\cdots\text{V}=\text{O}$ interactions are often green because of the contribution of $n-\pi$ transitions associated with the C=N moiety coupled to the aromatic rings. Reduced Schiff base compounds often are polymeric in the solid state and manifest colors that go from light gray to brown. The

differences in colors between polymeric compounds are mainly due to $\text{V}-\text{O}_{\text{phenolate}}$ ligand-to-metal charge-transfer (LMCT) transitions, which will have λ_{max} that depends on the particular structural features of the phenolate moiety. These depend on whether the compound is a SB or a RSB, on whether there are or are not $\text{V}=\text{O}\cdots\text{V}=\text{O}$ interactions, and on steric and/or electronic effects of the phenolate substituents.

IR spectra of compounds **10–19** were measured. With the exception of **10** and **15**, all $\text{V}^{\text{IV}}\text{O}$ compounds present $\nu_{\text{V}=\text{O}}$ frequencies ranging from 930 to 992 cm^{-1} , which is indicative of a square-pyramidal or trigonal-bipyramidal structure in the solid state. The much lower $\nu_{\text{V}=\text{O}}$ frequencies, such as those exhibited by **10** and **15**, may be considered to indicate apical interactions between neighboring molecules that decrease the strength of the $\text{V}=\text{O}$ bond.⁹

Crystals of **13** suitable for single-crystal X-ray diffraction were grown from THF solution and the molecular structure of **13** is depicted in Figure 2, with relevant distances and angles being presented in Table 2. Compound **13** corresponds to a dinuclear structure, which constitutes, to our present knowledge, the first molecular structure of a chiral $\text{V}^{\text{IV}}\text{O}$ compound belonging to this class determined by single-crystal X-ray diffraction. The absolute configuration at the stereogenic carbon atoms C2 and C18 is *S*. The metal centers are also chiral, with both V1 and V2 having a *C* absolute configuration. The configuration of a similar structure was obtained earlier by Pecoraro and co-workers for their nonchiral $[\text{V}^{\text{IV}}\text{O}(\text{SALAHE})_2]$ compound²⁷ [SALAHE = *N*-(hydroxyethyl)salicylideneamine]. The structure of **13** is notable for the following: (i) both square-pyramidal $\text{V}^{\text{IV}}\text{O}$ centers are syn-orthogonal to each other, contrary to the expected anti orientation; (ii) V–V has relatively short distance of 3.053(9) Å, which is close to the range admitted for a V–V single bond (2.459–2.970 Å).²⁸ One possible consequence of the proximity and orthogonal orientation of both square-pyramidal $\text{V}^{\text{IV}}\text{O}$ centers is the direct σ overlap of the d_{xy} orbitals, which can facilitate antiferromagnetic spin–spin coupling, yielding no EPR signal in solution. In solution, the orientation of the $\text{V}^{\text{IV}}\text{O}$ centers may be subject to change.

These observations are analogous with those made by other authors regarding dimeric and polymeric compounds with edge-sharing orthogonal $[\text{V}^{\text{IV}}\text{O}(\mu\text{-RO})_2\text{V}^{\text{IV}}\text{O}]$ cores.²⁹ It is expected that a similar dimeric structure is adopted by **17**, considering that it is EPR-silent. The V–O bonds V1–O3 and V2–O6 exhibit lengths typical of $\text{V}=\text{O}$ double bonds in pentacoordinated $\text{V}^{\text{IV}}\text{O}$ species [1.595(3) and 1.594(3) Å, respectively]. The $\text{V}-\text{O}_{\text{phenolate}}$ bonds V1–O1 and V2–O4 are significantly longer [1.901(3) and 1.910(3) Å, respectively] but similar to literature reports of phenolate-bound $\text{V}^{\text{IV}}\text{O}$ species.^{30,31} The V– N_{imine} bond lengths are in line with what is reported for related $\text{V}^{\text{IV}}\text{O}$ (Schiff base) compounds.^{30,32,33} In addition, both $\text{V}^{\text{IV}}\text{O}$ centers protrude noticeably from the $[\text{N}_{\text{imine}}, \text{O}_{\text{ArO}}, \text{O}_{\text{RO}}, \text{O}_{\text{RO}}]$ basal plane by 0.673 and 0.652 Å, respectively, indicative of strain on the five- and six-membered chelate rings, which is likely a result of the structural rigidity of the Schiff base ligand. The relevant bond angles are similar to what was reported for similar compounds.³⁰ The $\text{O}=\text{V}-\text{V}$ angles O3–V1–V2 and O6–V2–V1 differ slightly from each other by ca. 2°.

The $\text{V}^{\text{IV}}\text{O}$ complexes **10–12** and **14** were initially prepared according to literature procedures, which employ $\text{V}^{\text{IV}}\text{OCl}_2$ as the metal precursor.⁹ The elemental analyses of the aforementioned compounds are consistent with the expected

Table 2. Selected Structural Parameters for 4, 8, and 13

distances/Å				angles/deg			
Compound 4							
O1–C1	1.408(3)	O2A–C12	1.415(3)	C10–N1–C2	118.35(16)	C13–C12–O2A	119.0(2)
N1–C10	1.507(3)	O2B–C16	1.437(6)	N1–C2–C1	111.86(16)	C11–C12–O2A	119.97(19)
N1–C2	1.515(2)			N1–C2–C3	109.85(16)	C15–C16–O2B	114.5(3)
				C1–C2–C3	113.42(18)	C11–C16–O2B	124.1(3)
Compound 8							
O1–C1	1.425(4)	O2–C16	1.362(4)	C2–N1–C10	115.2(3)	O1–C1–C2	112.8(3)
N1–C2	1.478(5)	C2–C1	1.497(5)	O2–C16–C11	116.6(4)	C11–C10–N1	116.1(4)
N1–C10	1.500(5)	C10–C11	1.499(6)	N1–C2–C1	107.7(3)	C16–C11–C10	120.3(4)
Compound 13·C ₄ H ₈ O							
V1–O3	1.595(3)	V2–O6	1.594(3)	O3–V1–O1	110.28(15)	O2–V1–N1	78.77(12)
V1–O1	1.901(3)	V2–O4	1.910(3)	O6–V2–O5	109.23(13)	O2–V2–N2	137.69(12)
V1–O2	1.971(3)	V2–O5	1.972(3)	O3–V1–O5	111.15(13)	O1–V1–V2	116.36(9)
V1–O5	1.977(3)	V2–O2	1.975(3)	O4–V2–O2	89.53(12)	O5–V2–V1	39.44(8)
V1–N1	2.057(3)	V2–N2	2.035(3)	O3–V1–N1	104.60(14)	N1–V1–V2	112.90(9)
V1–[NOOO] ^a	0.673(15)	V2–[NOOO] ^a	0.652(16)	O4–V2–N2	88.01(13)	O3–V1–O2	114.07(14)
V1–V2	3.053(9)			O5–V1–N1	143.12(12)	O4–V2–O5	143.57(13)
				O6–V2–V1	117.89(11)	O1–V1–O5	88.79(11)
				O2–V1–V2	39.37(8)	O5–V2–O2	78.71(11)
				O2–V2–V1	39.28(8)	O1–V1–N1	87.22(14)
				O6–V2–O4	107.12(14)	O5–V2–N2	78.61(12)
				O1–V1–O2	135.51(12)	O3–V1–V2	120.08(11)
				O6–V2–O2	112.78(13)	O4–V2–V1	120.75(9)
				O2–V1–O5	78.69(11)	O5–V1–V2	39.32(8)
				O6–V2–N2	108.27(14)	N2–V2–V1	110.41(9)

^aDistance of the vanadium atom to the least mean squares of the equatorial donors.

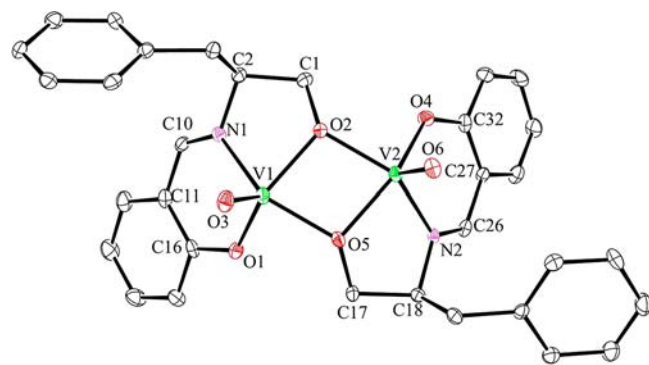


Figure 2. ORTEP diagram of 13 using 30% probability ellipsoids. Hydrogen atoms and the THF solvent molecule are omitted for clarity. The configuration at C2 and C18 is S, while at V1 and V2, it is C.

[ML]₂ formulation. The preparation methods using V^{IV}O(acac)₂ were employed as an approximation to the in situ generation of the V^{IV}O/V^V catalysts reported by Bolm and Bienewald.¹ Surprisingly, it was found that a minor adjustment to the V^{IV}O(acac)₂ procedure could lead to quite different products. Indeed, the V^{IV}O complexes derived from 6 and 7 are notable examples of this because inducing precipitation with an excess of water would lead to the formation of compounds with a [ML]₂ formulation, e.g., 15 and 17. In contrast, the use of both *n*-hexane and water gave compound 16 with the [ML]₂ formulation. This may be an important clue regarding the likely nature of the V^{IV}O/V^V compounds in solution, considering that the in situ species generated using the Bolm and Bienewald procedure are exposed to hundred-fold excesses of water during the catalytic experiments. In light of this, compound 12 was prepared a second time using this alternative procedure, along

with 13, its Schiff base variant. At a first observation, the precipitating solvent appears to be important in determining the end product ([ML]₂ vs [ML]₂), but compound 16 was obtained as a [ML]₂ species using either water or hexane, as stated above. Steric hindrance may play a role, but it is not clear how it affects the end product. Apart from the differences in the metal precursor used, the VOCl₂ method uses KOH, whereas the VO(acac)₂ method uses no additional base. It may be that at pH 8 deprotonation of the ligand alcohol group is favored and coordination of the alkoxido donor to the metal center is maintained even in the presence of large amounts of water as long as the pH is kept basic. In the VO(acac)₂ method, because there is no additional base to maintain a basic pH, protonation of the alkoxido donor may be favored instead, leading to VOL₂ species such as 15 and 17. In the case of 16, steric hindrance may prevent protonation of the alkoxido donor, thus leading to formation of the [VO(L)]₂ species even in the presence of water.

Characterization of the products obtained was made by resorting mainly to EPR, CD, UV–vis, and IR spectroscopy and elemental analysis. ⁵¹V NMR experiments were carried out in some cases to characterize the respective V^V species resulting from aerobic oxidation and to study their interaction with hydrogen peroxide.

EPR Spectra. Tridentate V^{IV}O(AOSB) and V^{IV}O(AORSB) complexes are known to form dinuclear or even polynuclear species in the solid state as well as in solution.^{34–36}

Solutions of the V^{IV}O complexes were analyzed by EPR at 77 K. For the dinuclear complexes prepared, the spin coupling between the two V^{IV}O centers depends on their relative orientation, but probably relatively strong antiferromagnetic exchange interactions are operating in all cases. Thus, because of both (i) the dinuclear nature of many of the compounds

and/or (ii) oxidation to V^V species, the solutions can either be EPR-silent or depict relatively low intensity signals.

Compounds **13** and **17** gave weak or no EPR signals in dichloromethane (DCM), *N,N*-dimethylformamide (DMF), and ethanol. A strongly coordinating solvent was required in some cases to break the antiferromagnetically coupled $V^{IV}O$ dinuclear structures apart, or at least weaken the $V-V$ interaction, if an appreciable EPR signal was to be detected. Thus, suitable spectra to allow determination of spin-Hamiltonian parameters were obtained in several cases, and Figure 3 shows the frozen solution X-band EPR spectra of **10**–

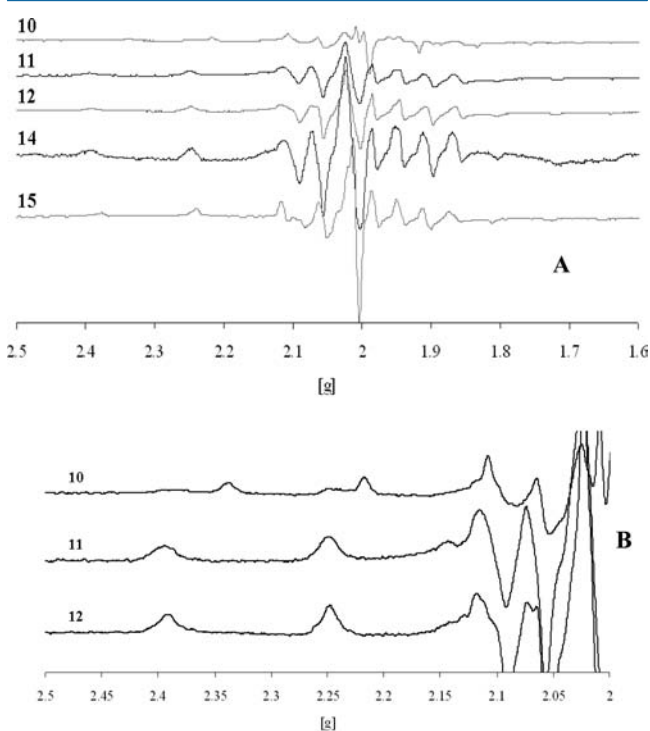


Figure 3. (A) First derivatives of the X-band EPR spectra of **10**–**12**, **14** (in DMF), and **15** (in EtOH) recorded at 77 K. (B) Amplification of the lower-field region of the X-band EPR spectra of **10**–**12** emphasizing the noticeable differences between **10** and **11/12**.

12, **14**, and **15** in DMF or ethanol solutions at 77 K. It is probable that in most cases the EPR signals recorded in solution for the dinuclear compounds correspond to their $V^{IV}O$ monomeric counterparts formed by solvolysis of the dinuclear complexes.

The EPR spectra depicted in Figure 3 present a well-defined hyperfine structure, and with the exception of **10**, all compounds yield similar EPR spectra. All A_z values were obtained after simulation with the appropriate software.¹⁰ The additivity rule developed by Wüthrich^{37a} and Chasteen et al.^{37b} $\{A_z^{\text{est}} = \sum A_{z,i} \text{ (} i = 1-4 \text{)},$ where $A_{z,i}$ are the contributions of each of the four equatorially coordinated donor groups} was applied so that the possible donor groups and binding modes in solution could be predicted. A secondary species with signals matching those of the remaining $V^{IV}O(\text{AORSB})$ complexes was detected in the EPR spectrum of **10**. Table 3 lists the calculated spin-Hamiltonian parameters, and Scheme 3 (and also Scheme SI-1 in the Supporting Information) depicts plausible binding modes, with the expected A_z^{est} values for each. The donor group contributions to A_z^{est} are as follows: $A_z(\text{O}_{\text{ROH}}) = A_z(\text{O}_{\text{H}_2\text{O}}) = 45.7 \times 10^{-4} \text{ cm}^{-1}$; $A_z(\text{O}_{\text{DMF}}) = 43.7$

Table 3. Experimental and DFT-Calculated (in Parentheses for **12'**, **13'**, **15'**, and **17'**; See Scheme 4) Spin-Hamiltonian Parameters for the Featured Tridentate $V^{IV}O(\text{AOSB})$ and $V^{IV}O(\text{AORSB})$ Complexes

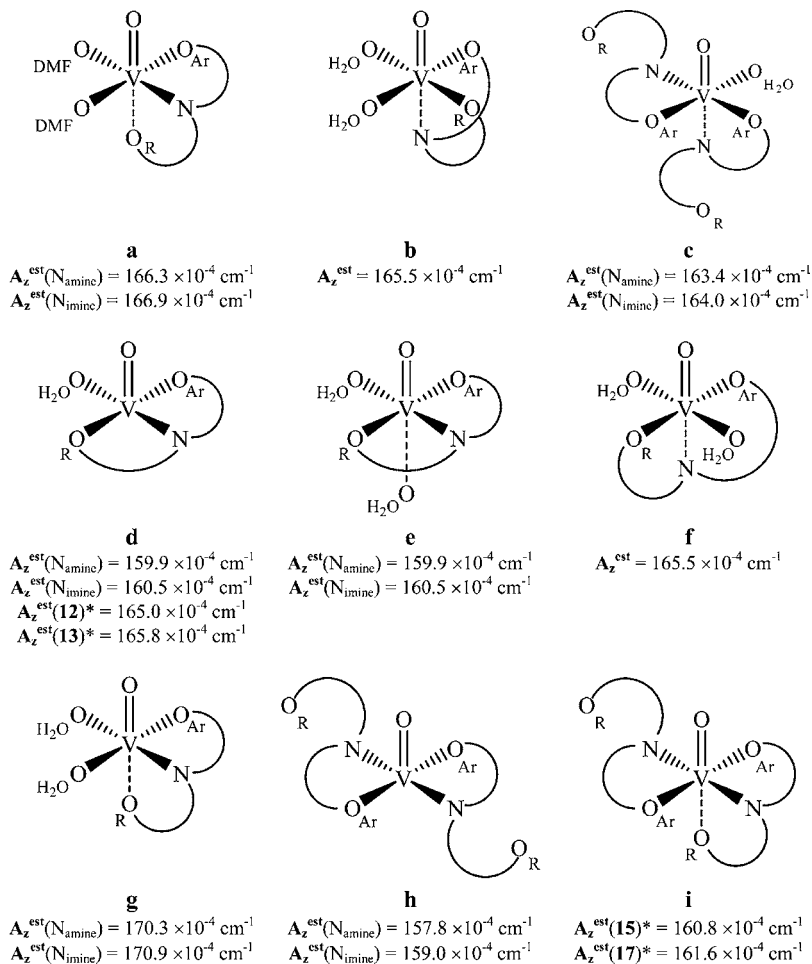
complex	g_x, g_y (or g_{\perp})	$ A_x , A_y $ (or $ A_{\perp} $) $\times 10^{-4} \text{ cm}^{-1}$	g_z (or g_{\parallel})	$ A_x $ (or $ A_{\parallel} $) $\times 10^{-4} \text{ cm}^{-1}$
10^a			1.962	149.0
10^b				165.0 ^c
11^a	1.979, 1.987	59.4, 60.6	1.948	168.5 (168.3) ^d
12^a	1.979, 1.984	57.6, 60.3	1.948	167.8
		12' (59.7, 62.2)		12' (165.0)
13		13' (59.8, 63.2)		13' (165.8)
14^a	1.979, 1.989	58.3, 58.7	1.947	168.5 (168.3) ^d
15^c	1.983, 1.974	58.3, 58.7	1.951	163.9
		15' (55.3, 58.1)		15' (160.8)
16^a	1.976, 1.982	57.7, 62.9	1.948	168.2 (168.3) ^d
17		17' (54.9, 60.2)		17' (161.6)
18^a	1.979, 1.980	55.1, 61.6	1.947	166.3 (166.3) ^d
19^a	1.978, 1.975	55.5, 66.9	1.947	169.9 (168.9) ^d

^aSpectra of solutions in DMF were measured at 77 K. ^bSecondary species. Estimated value. ^cSpectra of solutions in ethanol were measured at 77 K. ^dClosest estimation obtained using the empirical "additivity rule".^{37,38} See the Supporting Information for all plausible binding modes.

$\times 10^{-4} \text{ cm}^{-1}$; $A_z(\text{N}_{\text{imine}}) = 40.7 \times 10^{-4} \text{ cm}^{-1}$; $A_z(\text{N}_{\text{amine}}) = 40.1 \times 10^{-4} \text{ cm}^{-1}$; $A_z(\text{O}_{\text{ArO}}) = 38.8 \times 10^{-4} \text{ cm}^{-1}$; $A_z(\text{O}_{\text{RO}}) = 35.6 \times 10^{-4} \text{ cm}^{-1}$.^{27,31b,33b} The equatorial donor group sets were considered also taking into account the elemental analysis results and the estimation accuracy of $\pm 3 \times 10^{-4} \text{ cm}^{-1}$.

The experimental $|A_z|$ obtained for all $[\text{ML}]_2$ species (**11**, **12**, **14**, **16**, **18**, and **19**) range from 166.3 to $169.9 \times 10^{-4} \text{ cm}^{-1}$, all suggesting a $(\text{O}_{\text{Ar}}, \text{N}_{\text{amine}}, 2\text{O}_{\text{DMF}})_{\text{equatorial}}$ donor group set (binding mode a), calculated using the additivity rule alone. Compound **15**, being more similar in structure to the $V^{IV}O$ -salen and -salan compounds studied earlier by our group,^{9a} exhibits a lower $|A_z|$ suggestive of a $(2\text{O}_{\text{Ar}}, \text{N}_{\text{amine}}, \text{O}_{\text{water}})_{\text{equatorial}}$ donor set (mode c), reminiscent of the *mer-fac* conformations usually exhibited by salen- and salan-type compounds, although the experimental $|A_z|$ is too high for the initially expected $(2\text{O}_{\text{Ar}}, 2\text{N}_{\text{amine}})_{\text{equatorial}}$ donor group set (mode h) to be assigned. The main species of **10** with a A_z value of $149 \times 10^{-4} \text{ cm}^{-1}$ may be assigned to a $V^{IV}O$ species with a binding set of $(\text{O}_{\text{Ar}}, \text{N}_{\text{amine}}, 2\text{O}_{\text{RO}})_{\text{equatorial}}$, which corresponds to $A_z^{\text{est}} = 150.1 \times 10^{-4} \text{ cm}^{-1}$, whereas the second species is assigned to binding mode a. The low A_z value of **10** may also be explained by strong coordination of a donor atom trans to $\text{V}=\text{O}$, which can cause a noticeable decrease in A_z .²⁶ Despite its usefulness, the additivity rule does not take into account the changes to $|A_z|$ that may be caused by geometrical distortion³⁹ or coordination of an additional solvent trans to the $\text{V}=\text{O}$ bond.

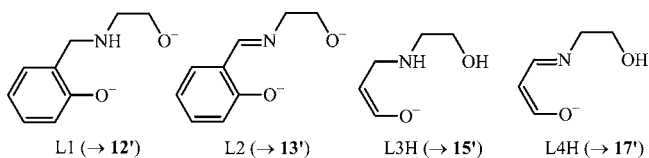
With the aim to interpret the experimental EPR data and to obtain some additional information about the composition and structural features of the vanadium complexes under study, quantum-chemical DFT calculations were carried out for the monomeric models $[\text{V}^{IV}O(\text{H}_2\text{O})_2\text{L1}]$ (**12'**) and $[\text{V}^{IV}O$ -

Scheme 3. Possible Binding Modes in Solution for the Prepared $V^{IV}O(AOSB)$ and $V^{IV}O(AORSB)$ Complexes^a

^aThe asterisk indicates DFT-calculated values. Globally, only binding sets d and h were found to be relevant (see the text).

(H_2O)₂L₂] (13') of 12 and 13 (see Scheme 4 for the model ligands L1, L2, L3H, and L4H).

Scheme 4. Molecular Models of Ligands Used for Quantum-Chemical DFT-Calculated EPR Parameter Predictions



First, calculations of various possible isomers of 12' and 13' were carried out, and the most stable isomers of these complexes were determined. The binding modes d–f were considered for 13', while the modes b and d–g were calculated for the more flexible 12'. The calculations indicated the following: (i) Structures 12'e, 12'g, and 13'e are predicted not to exist because no minima on the potential energy surface were found for these structures. All attempts of geometry optimization resulted in the extrusion of one water molecule from the inner coordination sphere and formation of the pentacoordinated complexes 12'd and 13'd (Figure 4TS in the Supporting Information). (ii) The most stable binding mode for both 12' and 13' is mode d with a geometry closer to trigonal-bipyramidal than to square-pyramidal. The structures

12'b, 12'f, and 13'f have significantly higher energies compared to 12'd or 13'd, respectively (by 83.7–105.4 kJ/mol in terms of ΔG ; a water molecule was added to the second coordination sphere of 12'd and 13'd to provide the same composition and, hence, the comparability of energies of all structures). (iii) Two conformers of 12'd (12'd1 and 12'd2; Figure 4) were found, and the former is by 20.1 kJ/mol more stable than the latter.

Second, DFT calculations of the EPR parameters were carried out for the most stable isomers of 12' and 13'. The calculated ⁵¹V hyperfine coupling constants are 165.0×10^{-4} and $165.8 \times 10^{-4} \text{ cm}^{-1}$ for 12'd1 and 13'd, respectively. The

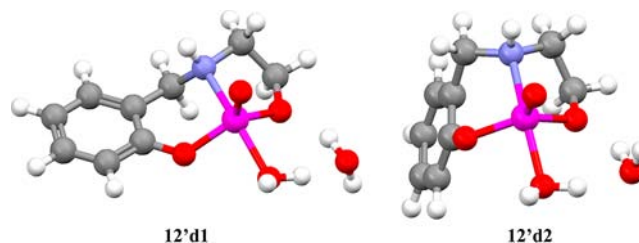
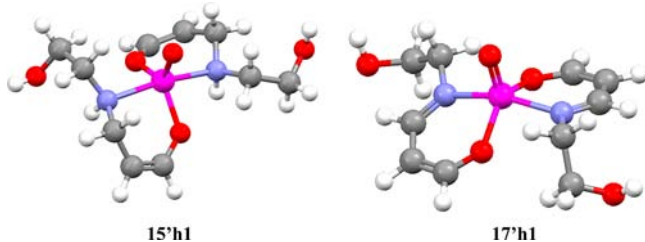


Figure 4. Equilibrium structures of 12'd1 and 12'd2. Conformer 12'd1 is more stable than 12'd2 by 20.1 kJ/mol, and the calculated $A_z = 165.0 \times 10^{-4} \text{ cm}^{-1}$. For 12'd1, the structural distortion parameter τ^{40} is 0.61, and for 12'd2, it is 0.67; therefore, 12'd1 is slightly more distorted toward a trigonal-bipyramidal geometry than 12'd2.

calculated values correlate well with the experimental data obtained for **12** (Table 3) and clearly support the d-type binding mode for **12**. No satisfactory EPR spectrum was obtained for solutions of **13** in both DMF and ethanol, but the DFT calculations and molecular structure obtained in the X-ray diffraction study anticipate that in solution the equatorial binding set should involve d-type O_{Ar} , N_{amine} , and O_{RO} binding modes.

Similar DFT calculations were also carried out for the model compounds $[V^{IV}O(L3H)_2]$ (**15'**) and $[V^{IV}O(L4H)_2]$ (**17'**) of complexes **15** and **17**. Two binding modes, h and i, were considered for **15'**. The isomer **15'i** is considered not to exist because there is no minimum on the potential energy surface corresponding to this structure: cleavage of the axial V–O_H bond and transformation to **15'h** with a pentacoordinated trigonal-bipyramidal coordination sphere occur during geometry optimization (Figure 4TS in the Supporting Information). For complex **15'h**, three structures with different stereoconfigurations at the amine nitrogen atoms were calculated (**15'h1**, **15'h2**, and **15'h3**; Tables 1TS and 2TS in the Supporting Information), with **15'h1** being the most stable and **15'h2** and **15'h3** being less stable by 14.2 and 15.1 kJ/mol, respectively. The calculated ^{51}V hyperfine coupling constants are $160.8 \times 10^{-4} \text{ cm}^{-1}$ for **15'h1** and $161.6 \times 10^{-4} \text{ cm}^{-1}$ for **17'h1**. The first value is not far from the experimental one obtained for **15** ($163.9 \times 10^{-4} \text{ cm}^{-1}$). The lowest-energy calculated structures for **15** and **17** are shown in Scheme 5,

Scheme 5. Representation of the Lowest-Energy Calculated Structures of $V^{IV}OL_2$ -Type Complexes **15'h1 and **17'h1**^a**



^aFor **15'h1**, the structural distortion parameter $\tau^{39,40}$ is 0.83, and for **17'h1**, it is 0.49; therefore, the structure for the $V^{IV}O(AORSB)_2$ complex **15'h1** is much more distorted toward a trigonal-bipyramidal geometry than the $V^{IV}O(AOSB)_2$ compound **17'h1**.

along with the respective calculated τ parameters. No satisfactory EPR spectrum was obtained for solutions of **17** in both DMF and ethanol. Previous authors have explored the effect of trigonal-bipyramidal distortion on the observed A_z . Most notably, the groups of Cornman and Garribba observed that A_z decreased with increasing τ , which, in turn, increased the x and y anisotropy.³⁹ However, Garribba and Micera also noticed that a correlation between τ and A_z and/or the x and y anisotropy is tenuous at best in aminophenolate class compounds, similar to those presented herein: highly distorted structures may not give significantly lowered A_z or high x and y anisotropy. Indeed, $|A_x - A_y|$ does not exceed $6.5 \times 10^{-4} \text{ cm}^{-1}$, which means substantial signal overlap at the midfield regions, and A_z^{exp} is higher than $165 \times 10^{-4} \text{ cm}^{-1}$ for the majority of compounds studied herein. Therefore, as emphasized previously,^{26,33b,41} the prediction of EPR parameters by carrying out these calculations is important to properly assign the binding sets of the prepared $V^{IV}O$ compounds.

In a summary of the EPR data, globally the EPR results in solution for the isolated dinuclear compounds are consistent with the presence of $V^{IV}O$ species with binding modes corresponding to a $(O_{Ar}, N_{amine}/N_{imine}, 2 \times \text{solvent})$ donor set, according to the additivity rule, or a $(O_{Ar}, N_{amine}/N_{imine}, O_{RO}, \text{solvent})$ donor set with trigonal-bipyramidal distortion when DFT calculations are taken into account. Compounds **15** and **17** may present a $(2O_{Ar}, N_{amine}/N_{imine}, \text{solvent})$ donor group set, although DFT calculations point to a $(2O_{Ar}, 2N_{amine}/N_{imine})$ donor set also with trigonal-bipyramidal distortion.

CD and Visible Spectroscopy. Besides giving support to characterization of the $V^{IV}O$ complexes prepared, the objective of these studies is to observe the transition from V^{IV} to V^V and to ascertain whether V^V exists primarily as $V^VO_3^{3+}$ or $V^VO_2^+$. As result of the LMCT bands and of the tendency toward oxidation in solution exhibited by the prepared $V^{IV}O(AORSB)$ and $V^{IV}O(AOSB)$ compounds, detection/identification of the weak d–d electronic transitions of the $d^1 V^{IV}O$ species is not unambiguous in most cases. The weak d–d bands gradually disappear as oxidation takes place, and the strong and broad $O_{phenolate} - V^{IV}O p\pi - d\pi^*$ charge-transfer bands centered around 500–550 nm mask both d–d bands [band I, $d_{xy} \rightarrow d_{yz}, d_{xz}$; band II, $d_{xy} \rightarrow d_{x^2-y^2}$], which normally appear around 600–800 and 520–600 nm, respectively.^{42,43} Band III ($d_{xy} \rightarrow d_z^2$) probably appears at ca. 400 nm, but it is usually masked by the intense charge-transfer bands. The recorded visible and CD spectra for the $V^{IV}O(AORSB)$ compounds are shown in Figures 5 and 6. The visible and CD spectra for the

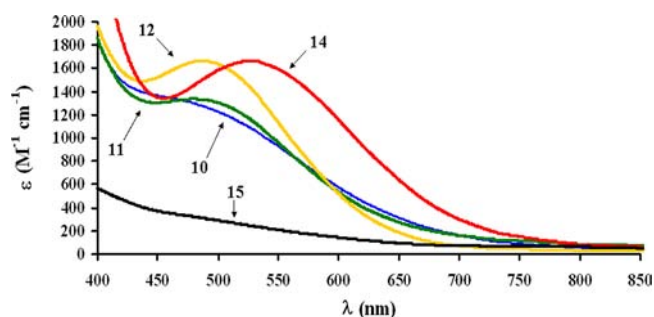


Figure 5. Isotropic visible spectra for $V^{IV}O(AORSB)$ compounds **10** (1.4 mM in ethyl acetate), **11** (1.5 mM in ethyl acetate), **12** (1.6 mM in ethyl acetate), **14** (1.1 mM in ethyl acetate), and **15** (1.1 mM in THF).

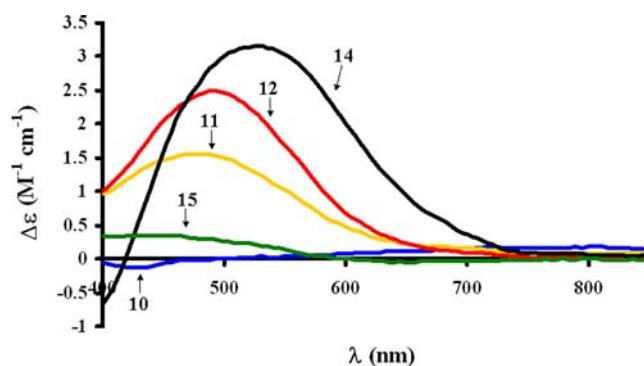


Figure 6. CD spectra of $V^{IV}O(AORSB)$ compounds **10** (1.4 mM in ethyl acetate), **11** (1.5 mM in ethyl acetate), **12** (1.6 mM in ethyl acetate), **14** (1.1 mM in ethyl acetate), and **15** (1.1 mM in THF).

$V^{IV}O(AOSB)$ compounds are included in the Supporting Information (see SI2). The relevant λ_{max} , molar absorptivity (ϵ), and molar CD ($\Delta\epsilon$) values obtained for the studied $V^{IV}O(AOSB)$ and $V^{IV}O(AORSB)$ compounds **10–15** and **17** are listed in Table 4.

Table 4. Data on Electronic Transitions in the Visible Range of 10–17 in Solution

compound	isotropic visible spectral data		CD spectral data	
	λ/nm	$\epsilon/M^{-1} cm^{-1}$	λ/nm	$\Delta\epsilon/M^{-1} cm^{-1}$
10	450 (sh)	1362	700–800	0.17
11	477	1335	480	1.55
12	487	1663	492	2.49
13	700 (sh)	30	714	-0.42
	520	118	548	1.13
14	527	1661	528	3.16
			440	0.34
15			650	-0.04
			708	-0.28
17	500 (sh)	810	540	0.79

The bands observed at ca. 450–550 nm for **10–12**, **14**, and **17** are assigned to $O_{phenolate}-V^V p\pi-d\pi^*$ charge-transfer bands.^{33b,44} With the exception of **13**, the d–d bands I and II could not be clearly identified because of oxidation and/or masking by the charge-transfer bands. In the case of **13**, only a weak band is discernible at ca. 520 nm ($\epsilon = 118 M^{-1} cm^{-1}$), assignable to a d–d (band II) transition (or containing contribution from band II), and a shoulder at ca. 700 nm ($\epsilon \approx 30 M^{-1} cm^{-1}$), assignable to band I. In the case of **10**, a weak positive band is also detected at ca. 650–850 nm.

Along with complex **17**, **13** also exhibited the azomethine ($C=N$) $n-\pi^*$ and $\pi-\pi^*$ transitions, which typically have λ_{max}

below 400 nm.³¹ Compound **15** gave a rather featureless spectrum, and no bands could be clearly identified for $\lambda > 400$ nm, although CD bands could be detected at 440, 650, and ~ 708 nm (Table 4).

Most of the compounds analyzed exhibit CD spectra in the visible range, and the optical activity associated with d–d transitions can be considered to be detected for **10**, **13**, **15**, and **17**. In these cases, weak d–d transitions (band I)⁴³ are visible in the 650–800 nm range. The bands observed around 400–600 nm probably include contributions of both charge-transfer and d–d band II.

In the CD spectra of **11**, **12**, and **14**, the d–d transitions are not clearly visible either because of oxidation or because they are too weak to be detected in the conditions used. However, rather strong bands observed around 400–600 nm are associated with charge-transfer bands.

The fact that both the d–d and $O_{phenolate}-V^V$ charge-transfer bands have associated optical activity is indicative of chirality at the metal center in addition to chiral induction from the ligand.^{31,33b,45} In addition, the amine nitrogen atom becomes a stereogenic center upon coordination. Many isomers are possible and several types of diastereomers are also possible for both the $[ML]_2$ and ML_2 formulations. Figure 7 shows endo/exo diastereomers that can arise from chiral-at-metal vanadium compounds, considering the $[ML]_2$ and ML_2 formulations. Therefore, the CD spectrum observed for each compound is the sum of the various chiral-at-metal stereoisomers present in different amounts (chiral-at-nitrogen, chiral-at-carbon, and chiral-at- V^{IV} or $-V^V$). Noteworthy are the very weak CD spectra of **10** and **15**. It is possible that these represent the case where almost racemic mixtures of chiral-at-metal and chiral-at-nitrogen species are present. As oxidation from V^{IV} to V^V took place, the solutions acquired an intense dark-red coloration with the exception of compound **15**, which yielded a yellow-orange coloration. Fresh solutions of **12**, **13**,

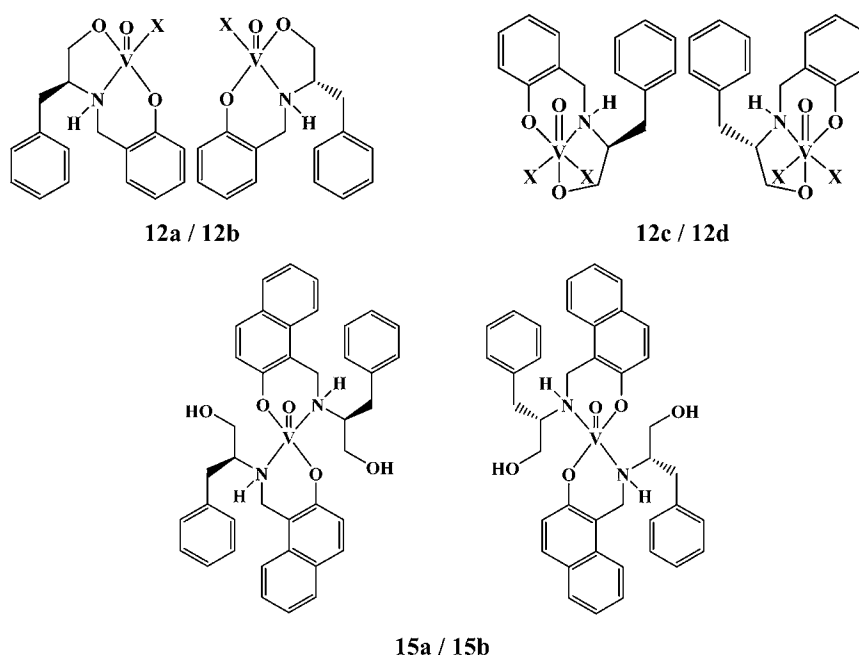


Figure 7. In all $V^{IV}O(AORSB)$ complexes depicted, the vanadium, α -carbon, and amine nitrogen atoms are stereogenic centers. Possible endo/exo diastereomers are shown for $V^{IV}O(AORSB)$ compounds with either a $[ML]_2$ or ML_2 formulation resulting from chirality-at-metal and at the α -carbon atom. The letter X denotes a coordinated solvent molecule. In these complexes, when the amine nitrogen atom coordinates, it also becomes a stereogenic center, but this is not the point emphasized in this figure.

15, and 17 were prepared, and the respective spectra were measured shortly after solution preparation and again after several days. The visible absorption spectra of compounds 12 and 13 are shown in Figures SI-3A and SI-3B in the Supporting Information. The spectra recorded of 15 and 17 are included in the Supporting Information (see Figures SI-3C and SI-4). The effect of oxidation on the optical activity was also followed by CD spectroscopy, and CD spectra were also measured immediately after preparation and several days after preparation of the $V^{IV}O(AORSB)$ and $V^{IV}O(AOSB)$ solutions. The CD spectra recorded for 12–15 and 17 are included in the Supporting Information (see SI-5 to SI-9). The relevant λ_{max} , molar absorptivity (ϵ), and molar CD ($\Delta\epsilon$) values are listed in Tables 5 and 6.

Table 5. Observed λ_{max} and ϵ Values for 12, 13, and 17 after Aerobic Oxidation

12			13			17		
λ / nm	t/h	ϵ/M^{-1} cm^{-1}	λ / nm	t/h	ϵ/M^{-1} cm^{-1}	λ / nm	t/h	ϵ/M^{-1} cm^{-1}
486	0.25	1663	496	0.25	497	500	0.25	318
	72	1663		192	1031		192	788

Table 6. Observed CD λ_{max} and $\Delta\epsilon$ Values for 10–14 and 17 after Aerobic Oxidation

10			11			12		
λ / nm	t/h	$\Delta\epsilon/M^{-1}$ cm^{-1}	λ / nm	t/h	$\Delta\epsilon/M^{-1}$ cm^{-1}	λ / nm	t/h	$\Delta\epsilon/M^{-1}$ cm^{-1}
748	0.25	0.17						
	72	−0.01						
536	0.25	0.02	476	0.25	1.56	492	0.25	2.49
	72	−0.33		72	1.60		72	2.65
13			14			17		
λ / nm	t/h	$\Delta\epsilon/M^{-1}$ cm^{-1}	λ / nm	t/h	$\Delta\epsilon/M^{-1}$ cm^{-1}	λ / nm	t/h	$\Delta\epsilon/M^{-1}$ cm^{-1}
712	0.25	−0.42				708	0.25	−0.28
	192	0.01					192	−0.06
536	0.25	1.31	516	0.25	3.13	540	0.25	0.69
	192	1.01		72	3.78		192	0.03

In all cases, a decrease in the absorbance values for $\lambda > 700$ nm (in some cases, $\lambda > 600$ nm) is observed and is consistent with the expected $V^{IV} \rightarrow V^V$ oxidation.

There was a very small change in the spectrum of 12 after 3 days, namely, for $\lambda > 650$ nm, indicating that no other process occurred after the initial oxidation; the d–d bands are too weak to be clearly distinguished, and the $V^{IV}O$ compound in solution was probably almost completely oxidized to V^V by the time the first spectrum was measured. In the case of 13 and 17, an increase in the intensity of the charge-transfer band centered at ca. 500 nm was observed after 8 days. The $V^{IV}O(AOSB)$ compounds appear to exhibit greater resistance to oxidation than the $V^{IV}O(AORSB)$ analogues, which allowed observation of the transition from V^{IV} to V^V , namely, by an increase in the intensity of the LMCT bands. Compound 15 followed the same trend, although this increase in intensity was not so pronounced and no bands could still be clearly identified. With the exception of 15, the solutions of 12, 13, and 17 acquired a strong red coloration because of the appearance of the

$O_{phenolate}-V^V p\pi-d\pi^*$ charge-transfer bands around ca. 500 nm. These red-shifted charge-transfer bands are suggestive of the existence of phenolate-bound V^VO^{3+} species, whereas the phenolate-bound $V^VO_2^+$ species normally exhibit these bands around 350–400 nm, hence the reported difference in coloration for both types of compounds.⁴³ Compound 15 may correspond to the latter case, considering the minor change of the band intensity in the 450–550 nm range. Overall, the experimental ϵ values for the bands around 450–550 nm are lower compared to those reported for V^V compounds with similar donor atom groups;^{9,44} this may indicate that the presence of a mixture of both V^VO^{3+} and $V^VO_2^+$ species is a more likely scenario in several of these solutions.

The CD spectra of compounds 11–13 and 15 showed some but not drastic changes several days after preparation of the solutions. The weak d–d bands at $\lambda > 650$ nm, when distinguished, tend to disappear, and there was a slight increase of the signal around 500–550 nm, assigned earlier to charge-transfer transitions.

The most notable changes were observed with the $V^{IV}O(AOSB)$ compounds 13 and 17: in the CD spectra taken 1 week after preparation of the respective solutions, the weak d–d band I observed at ca. 650–800 nm is no longer detected. In the particular case of 13, the charge-transfer band at ca. 520 nm remains mostly unaffected, while there is an increase of the signal intensity below 450 nm. For 17, no signals were detected above 500 nm 1 week after sample preparation. An increase of the signal intensity below this λ was also observed.

^{51}V NMR. Compounds 15 and 17 were used for ^{51}V NMR measurements, and their interaction with increasing amounts of hydrogen peroxide was evaluated. The sulfoxidation procedure initially reported by Bolm and Bienewald¹ employs aqueous H_2O_2 in hundred-fold excess relative to the catalyst. Given that it employs an excess of ligand, it is likely that ML_2 species form at some point in the reaction. Therefore, we chose to also employ ML_2 compounds 15 and 17 as models in this study. Additional studies using conditions very similar to those employed by Bolm and Bienewald were also made for comparative purposes.

Solutions (2 mM) of the above compounds in DCM were prepared 4 h prior to the ^{51}V NMR measurements. To ensure a homogeneous medium after the successive additions of oxidant, a 0.39 M solution of aqueous H_2O_2 in acetone was used. After the first measurement, controlled molar equivalents of H_2O_2 were successively added, and NMR spectra were measured between additions. Figure 8 shows the spectra obtained for 17. Unexpectedly, 15 did not yield adequate NMR spectra because no peaks were observed during the experiment. Initially, in the case of 17, five species can be observed at −510, −518, −526, −537, and −551 ppm, with the latter three signals being the three major ones. These three signals may be assigned to $V^VO_2^+$ species (species A and B; see Scheme 6) by a comparison with data reported in the literature for tridentate $[V^VO_2(HL)]$ compounds bearing mixed nitrogen and oxygen donor groups.⁴⁶ An alternative possibility is to consider the phenolate-bound ML_2 formulation of 17, in which the signals at −526, −537, and −551 ppm could be due to conformational isomers of μ -oxido V^VO^{3+} species (e.g., E–G in Scheme 6). It was reported that alkoxido $V^VO[N,N,O,O]$ species may exhibit distinct chemical shifts depending on the donor atoms cis or trans to the $V=O$ bond.⁴⁷ It is possible that this could also be extended to μ -oxido $V^VO[N,N,O,O]$ species. Moreover, the

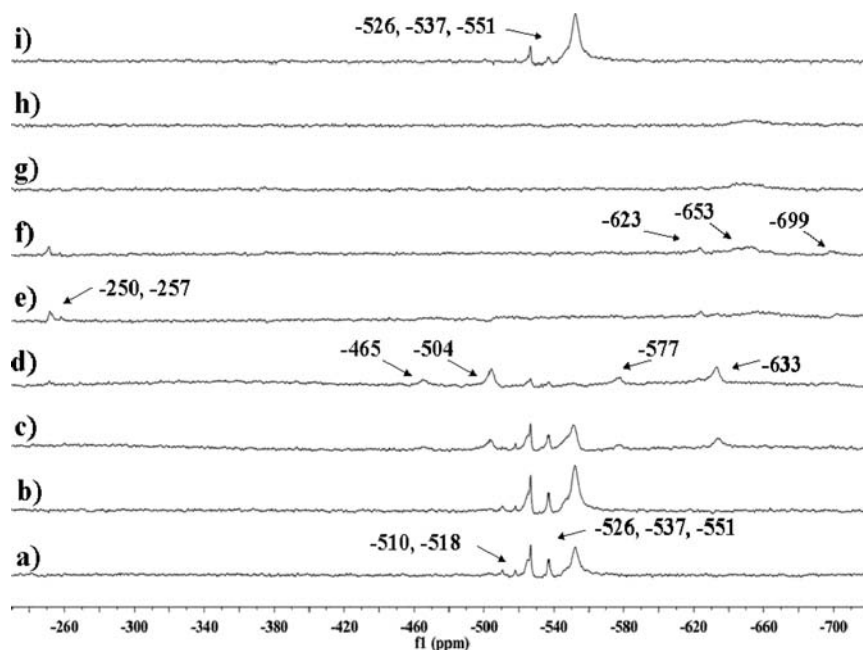
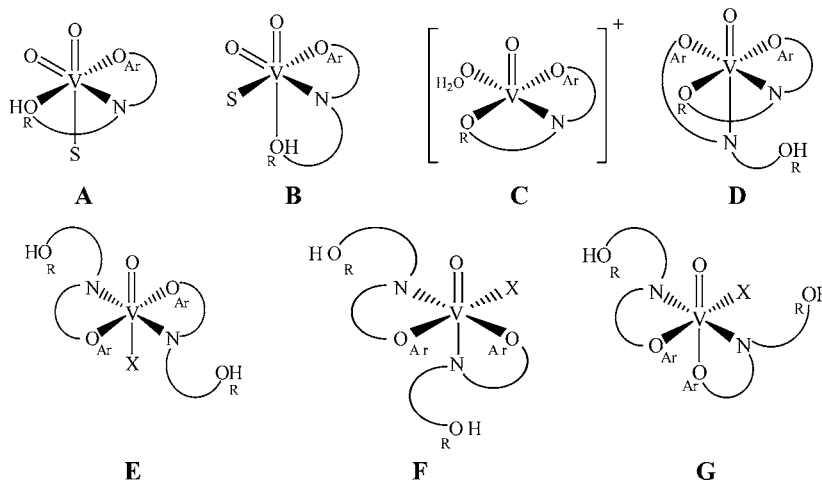


Figure 8. ^{51}V NMR spectra of **17** after consecutive additions of H_2O_2 in CD_2Cl_2 : (a) 6 h after preparation of the solution and no H_2O_2 added; (b) 0.5 equiv of H_2O_2 ; (c) 1 equiv (total) of H_2O_2 ; (d) 2 equiv (total) of H_2O_2 ; (e) 4 equiv (total) of H_2O_2 ; (f) 5 equiv (total) of H_2O_2 ; (g) 10 equiv (total) of H_2O_2 ; (h) 15 equiv (total) of H_2O_2 ; (i) 1 h after the last addition of H_2O_2 .

Scheme 6. Proposed V^{V} Species Present in CH_2Cl_2 Solution of **17 upon Additions of H_2O_2 in CD_2Cl_2 ^a**



^aThe letters S and X denote a solvent molecule and a μ -oxido group, respectively.

major chemical shifts observed for **17** are consistent with data reported in the literature for similar $\text{V}^{\text{V}}\text{O}$ compounds bearing the $[\text{N},\text{N},\text{O},\text{O}]$ donor set, namely, salen- and salan-type compounds.⁹ Another factor to keep in mind is that steric bulk may affect the ^{51}V chemical shifts. $\text{V}^{\text{V}}\text{O}[\text{N},\text{N},\text{O},\text{O}]$ species bearing an additional alkoxido ligand typically exhibit shifts at lower fields than the μ -oxido variants, with this having been mostly attributed to the decreased bulk around the metal core.⁴⁸

To assist in the ^{51}V NMR assignments, quantum-chemical DFT calculations were carried out with simplified models also to predict probable chemical shifts. The calculations indicate that the charged ML -type species **C** and the neutral ML_2 -type species **D** (both $\text{V}^{\text{V}}\text{O}^{3+}$ species) should exhibit chemical shifts of -498 and -503 ppm, respectively, which are significantly further downfield from the observed major species at -526 ,

-537 , and -551 ppm. Taking into account these calculations and the fact that $\text{V}^{\text{V}}\text{O}^{3+}$ centers appear to be associated with polyanionic ligands of higher denticity such as the diaminebis(phenolates),^{9,44,47} we propose that the observed major peaks correspond to $\text{V}^{\text{V}}\text{O}_2$ complexes (e.g., **A** and **B**),⁴⁹ with the $\text{V}^{\text{V}}\text{O}^{3+}$ compounds accounting for the minor peaks.

The first additions of H_2O_2 correspond to an apparent increase in the relative intensity of the signal at -551 ppm. Upon the addition of 1 equiv of H_2O_2 , additional signals at ca. -465 , -504 , -577 , and -633 ppm were clearly visible. The addition of another 1 equiv of oxidant resulted in a drastic decrease of the signals initially observed at -526 , -537 , and -551 ppm. The signals at -465 and -504 ppm may be due to the presence of $[\text{V}^{\text{V}}\text{O}(\text{L}_2)]$ species such as **D** (Scheme 6).

The signals at -577 and -633 ppm are within the expected range for $[\text{V}^{\text{V}}\text{O}(\text{O}_2)\text{L}]$ -type species.^{30,50} After the addition of 5

Table 7. Sulfoxidation of Thioanisole with the VO^{IV}(AOSB) and VO^{IV}(AORSB) Catalysts^a

entry	catalyst	solvent	T/°C	t/h	conv/% ^c	ee/% ^d	sulfoxide yield/%	sulfone yield/%
1		DCE	25	24	9	0	9	0
2		acetone	25	24	3	0	3	0
3		EtOAc	25	24	2	0	2	0
4		CH ₃ CN	25	24	2	0	2	0
5	10	DCE	0	24	15	0	15	0
6	10	CH ₂ Cl ₂	0	24	15	8(S)	15	0
7 ^b	10	CH ₂ Cl ₂	25	4	60	0	53	7
8	10	CH ₃ CN	0	24	80	0	68	12
9 ^b	11	DCE	40	4	71	6(S)	63	8
10 ^b	11	CH ₂ Cl ₂	25	4	66	5(S)	60	6
11	11	CH ₂ Cl ₂	0	24	26	0	25	1
12	11	CHCl ₃	0	24	73	3(S)	69	4
13	11	CH ₃ CN	0	24	99	0	90	9
14 ^b	12	CH ₂ Cl ₂	0	24	68	4(S)	61	7
15	12	CH ₂ Cl ₂	25	4	91	1(S)	83	8
16 ^b	14	DCE	40	4	76	11(S)	65	11
17	14	CH ₂ Cl ₂	0	24	93	6(S)	82	11
18 ^b	14	CH ₂ Cl ₂	25	4	79	9(S)	67	12
19	14	CHCl ₃	0	24	93	9(S)	88	5
20	15	CH ₂ Cl ₂	0	24	4	0	4	0
21	15	acetone	0	24	0	0	0	0
22	16	CH ₂ Cl ₂	0	24	98	57(S)	92	6
23	17	CH ₂ Cl ₂	0	24	91	60(S)	87	4
24	17	acetone	0	24	99	7(S)	94	5
25	18	CH ₂ Cl ₂	0	24	89	10(S)	75	14
26	19	CH ₂ Cl ₂	0	24	97	59(S)	92	5

^aConditions: *n*S = 1 mmol; *n*H₂O₂:*n*S = 1.5; 1 mol % of catalyst. ^b*n*H₂O₂:*n*S = 1.05. ^cConversion percentage refers to the amount of thioanisole consumed to produce both the sulfoxide and sulfone. ^dEnantiomeric excess determined by chiral HPLC.

equiv of oxidant, the aforementioned signals almost disappear and downfield bands at ca. -250 and 257 ppm and broad high-field resonances at ca. -623, -653, and -699 ppm are detected. The signals at -250 and -257 ppm fall outside the expected range for V^V compounds with mixed nitrogen and oxygen donor sets; such downfield shifts are typical of V^V species containing polarizable ligands such as chlorides, bromides, and thiolates.⁴⁸ Given that such species are not present in solution, the observed signals must then be a manifestation of not easily predicted changes in the electronic properties of the ligand, possibly of the type seen for noninnocent ligands, such as catecholates.⁵¹ It was also reported that both imines and phenolates can be redox-active, and under these conditions, quinone-type species may be formed, which can interfere with the behavior of the coordinated metal centers.⁵² The signals at -623 and -653 ppm may be assigned to [V^VO(O₂)]-type species, while the signal at -699 ppm is probably due to the presence of [V^VO(O₂)₂]-type compounds.⁵³

After the addition of 15 equiv of oxidant, only the broad signal at -653 ppm remained. It is possible that precipitation of small particles of the V NMR active species has occurred, but because the solution had a very dark color, this was not clearly confirmed. Interestingly, the major species observed initially at -526, -537, and -551 ppm were regenerated ~60 min after the last addition of oxidant. This indicates that these peroxido species are relatively short-lived and that after their degradation the initial V^V species are regenerated. A similar result was obtained after the addition of 10 equiv of thioanisole following the addition of an equal amount of oxidant. Experiments made using in situ generated 17 according to the procedure by Bolm

and Bienewald [V^{IV}O(acac)₂-to-ligand ratio of 1:1.5] yielded similar results, although the initial peak intensities differed. The spectra obtained for these cases are included in the Supporting Information (Figures SI-12 and SI-13).

The experiments made with in situ generated 15 showed less variety of ⁵¹V NMR peaks. Three weak peaks at -463, -474, and -509 ppm were initially observed and probably correspond to V^VOL complexes. Upon the addition of 10 equiv of oxidant, these signals disappeared and a weak but discernible signal at -709 ppm was observed, indicative of the formation of [V^VO(O₂)₂]-type species. The addition of thioanisole did not induce regeneration of the initial species and no ⁵¹V NMR signals were observed afterward, probably partly because of reduction of all V^V species to V^{IV} compounds. Noteworthy was the slight turbidity of the sample solutions of 15 after the addition of oxidant. Precipitation of the NMR-active species out of solution may be the most likely cause for the nondetection of ⁵¹V NMR sharp signals; it is known that V^V species tend to form colloidal chain polymers that yield broad and weak NMR signals at best.⁵⁴

Catalytic Experiments. The prepared V^{IV}O(AORSB) compounds were screened for their catalytic potential in the asymmetric sulfoxidation of thioanisole under a variety of conditions. Various solvents were used such as CH₂Cl₂, CHCl₃, 1,2-dichloroethane (DCE), acetone, ethyl acetate, and acetonitrile. In all cases, the final products were either (*R*)- or (*S*)-methyl phenyl sulfoxide or sulfone. The results obtained are presented in Table 7.

Contrary to what were our initial expectations by a comparison with the V^VO(salan) systems,⁹ the V^{IV}O(AORSB) catalysts exhibited low enantioselectivities, despite good

conversions and low sulfone amounts. The reaction temperature seemed to have little effect on the observed enantioselectivity, although there was a slight increase in the enantiomeric excess with higher temperature in the case of **11** (entries 9–11) and **14** (entries 16–18). The solvent manifested effects mainly in the degree of conversion. For instance, for **10**, the reaction run in acetonitrile gave no enantiomeric excess (entry 7) but gave higher conversions compared to the reaction in chlorinated solvents at the same temperature. In fact, the reactions in DCE and CH₂Cl₂ at 0 °C gave low conversions (entries 5 and 6), but low enantiomeric excess was observed only in CH₂Cl₂ (entry 6). The same trend in terms of conversion was observed for **11**, although the reaction in CH₂Cl₂ at 0 °C gave a slightly higher conversion (entry 11). **12** exhibited a higher activity in CH₂Cl₂ and a slightly higher enantioselectivity than **11** at the same temperature (entry 14). The increase in the reaction temperature was accompanied with a significant increase in conversion without additional sulfone production (entry 15).

Catalyst precursor **14** gave the best results in terms of activity and enantioselectivity. At 0 °C in CH₂Cl₂, a conversion of 93% and an enantiomeric excess of 6% was obtained along with 11% of sulfone (entry 17). Replacement of CH₂Cl₂ by CHCl₃ caused a slight increase in enantiomeric excess from 6 to 9% and a reduction in sulfone production (entry 19). Increasing the temperature resulted in an additional increase in enantioselectivity when using DCE as solvent (entry 16). Compound **15** followed the same trend as the other V^{IV}O(AORSB) compounds and exhibited very low activity and enantioselectivity (entry 20), contrasting with the much higher conversion and enantiomeric excess given by the V^{IV}O(AOSB) analogue **16** (entry 16). Using acetone instead of DCM did not produce any noticeable changes in both the activity and enantioselectivity of **15** (entry 21). Notable is the similarity of the results obtained with either V^{IV}O(AOSB) compounds **16** and **17** (entries 22 and 23). This may imply that the asymmetric transition state in both cases is the same, regardless of their initial formulation (**16** is a dinuclear [ML]₂ complex, while **17** is the corresponding ML₂ monomer).

Changing the solvent to acetone proved detrimental to the enantioselectivity of **17**, leaving the activity unaffected (entry 24). The best results in terms of conversion and enantiomeric excess were obtained with the *o*-vanillin derivatives **18** and **19**. The V^{IV}O(AORSB) compound **18** gave a high conversion, although the enantiomeric excess did not surpass 10% (entry 25), while the corresponding V^{IV}O(AOSB) compound **19** gave a very high conversion and an enantiomeric excess close to 60% (entry 26).

The obtained enantiomeric excesses for the various V^{IV}O(AORSB) catalysts are low and did not go beyond 11%. These results indicate that the C=N double bond present in the ligand structure of Bolm's original catalyst plays a relevant role as far as the enantioselectivity of the catalytic species is concerned. This may result from both the rigidity conferred by the C=N double bond and the fact that in the AORSB compounds the amine nitrogen donor atoms become stereogenic centers upon coordination, probably yielding an almost racemic mixture [containing ~50% of (*S*)-N_{amine} and ~50% of (*R*)-N_{amine}], this may contribute to the decrease in the enantioselectivity for sulfoxidation.

The in situ versions of the prepared V^{IV}O(AORSB) catalysts were also tested in the asymmetric sulfoxidation of thioanisole. The Schiff base ligand precursor compounds **5** and **7** were

included in this study to observe whether the C=N double bond indeed plays such a determinant role in the catalyst enantioselectivity. The experimental conditions follow the protocol employed by Bolm and Bienewald,¹ and the results obtained are presented in Table 8.

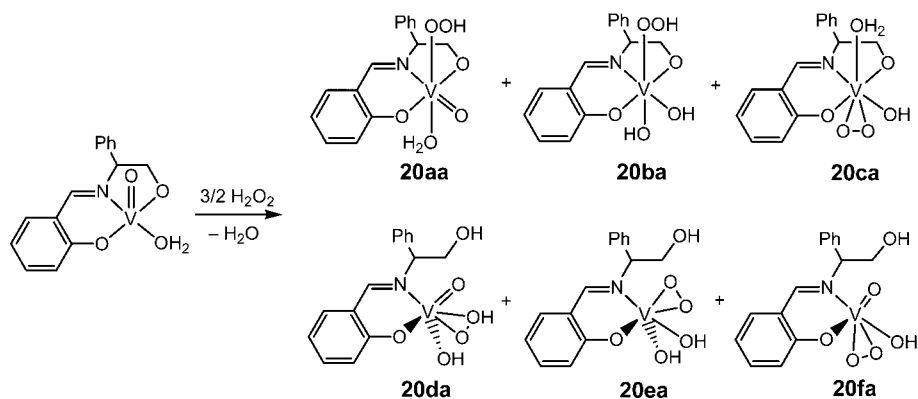
Table 8. Sulfoxidation of Thioanisole with in Situ V^{IV}O(AOSB) and V^{IV}O(AORSB) Procedures^a

entry	catalyst	conv/ % ^d	ee/% ^e	sulfoxide yield/%	sulfone yield/%
1	V ^{IV} O(acac) ₂ /1	5	15(S)	5	0
2	V ^{IV} O(acac) ₂ /2	3	0	3	0
3	V ^{IV} O(acac) ₂ /3	5	5(S)	5	0
4	V ^{IV} O(acac) ₂ /4	77	6(S)	61	16
5	V ^{IV} O(acac) ₂ /5	90	42(S)	82	8
6	V ^{IV} O(acac) ₂ /6	34	0	33	1
7 ^b	V ^{IV} O(acac) ₂ /6	42	0	41	1
8	V ^{IV} O(acac) ₂ /7	84	50(S)	81	3
9 ^c	V ^{IV} O(acac) ₂ /7	94	3(S)	83	11
10	V ^{IV} O(acac) ₂ /8	93	2(S)	83	10
11	V ^{IV} O(acac) ₂ /9	96	58(S)	90	6

^aConditions: 2 mL of CH₂Cl₂; *n*S = 1 mmol; *n*H₂O₂:*n*S = 1.2; 1 mol % of V^{IV}O(acac)₂; 1.5 mol % of ligand; *T* = 0 °C; *t* = 24 h. ^bReaction carried out in ethyl acetate. ^cReaction carried out in ethyl acetate at room temperature. ^dConversion percentage refers to the quantity of thioanisole consumed to produce both the sulfoxide and sulfone. ^eEnantiomeric excess determined by chiral HPLC.

The in situ versions of **10**–**12** (entries 1–3, respectively) gave even lower activities than when the prepared catalyst precursor versions were used, and only the in situ version of **14** exhibited a comparable activity and enantioselectivity at the same temperature and in the same solvent (entry 4). When the Schiff base version of **14** was used, a significant increase in the enantioselectivity was obtained (from 6 to 42%, entry 5), with this result being coherent with those reported by Zhao and co-workers.⁵⁵ Structurally, the difference resides only in the type of C–N bond bridging the amino alcohol and phenolate moieties. Besides the probable formation of approximately equal amounts of (*S*)-N_{amine} and (*R*)-N_{amine} stereoisomers, the double bond present in the latter confers rigidity to the ligand structure apparently also necessary for adequate asymmetric induction in sulfoxidation of thioanisole. If this C=N double bond is replaced by a C–N single bond, as is the case of **4**, a more flexible ligand structure is obtained, with this being detrimental not only to the catalyst enantioselectivity but to the overall activity. A similar behavior was observed when the 2-hydroxynaphthaldehyde derivatives **6** and **7** were used as ligand precursors. Again, the reaction run with the Schiff base ligand precursor **7** gave significantly higher enantiomeric excess in DCM compared to the reaction run using the respective reduced Schiff base compound **6** (entries 6 and 8). Using ethyl acetate as the solvent at room temperature resulted in a drastic drop in the enantioselectivity with **7** as the ligand, but an increase in conversion was observed for both **6** and **7** (entries 7 and 9).

The in situ catalysts prepared from compounds **8** and **9** gave results very similar to those obtained with catalyst precursors **18** and **19** (entries 10 and 11). The phenolate moiety substituents appear to have a relatively minor role in the overall enantioselectivity. Compounds **5** and **7** have quite different phenolate moieties, yet **5** with a *tert*-butyl group ortho

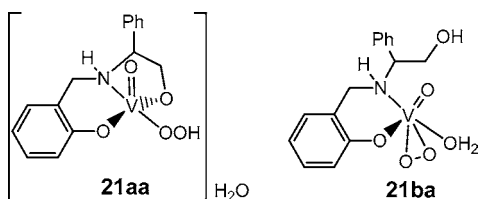
Scheme 7. Possible Isomeric V^V Peroxido Complexes Derived from Model Compound 20 (Only the Most Stable Isomers Are Indicated)

to the phenolate functionality yielded slightly lower enantiomeric excess compared to 7, which has no bulky alkyl group substituents in that position. In turn, compound 9 with a *o*-methoxy group gave the best results in terms of enantioselectivity, slightly better than those obtained with 5 and 7. This contrasts with what was reported for tetradentate V^{IV}O(salen) and V^{IV}O(salan), where phenolate substituents are determinant in the overall enantioselectivity.^{2,9} In light of the present results, an excess of ligand generally employed in the in situ procedures can be considered unnecessary when the in situ catalyst enantioselectivities are compared with those exhibited by prepared V^{IV}O(AOSB) precatalysts.

Theoretical Mechanistic Study. In this section, results of the theoretical DFT calculations of the mechanism of thioanisole sulfoxidation with two vanadium catalysts are discussed. The V^{IV} complexes used in the experimental part are unstable in the presence of H₂O₂ and are easily oxidized to the corresponding V^V peroxido species (see Scheme 7 for the phenyl-substituted model 20 with *R* configuration on the chiral carbon atom). First, various possible isomers of 20 with different localizations of the proton (20a–20f) were calculated, and their relative stabilities were estimated. Each of the complexes 20a–20f, in turn, has several isomers with different mutual positions of the ligand in the coordination sphere of the metal (see Figure 1TS in the Supporting Information for the structures and energy values). The calculations of all of these isomers indicated that the most stable one is the hexacoordinated oxidoperoxido complex 20fa (considering that the peroxido ligand occupies two coordination positions) with the protonated imino alcohol ligand (see Figure 1TS in the Supporting Information for the energy values).

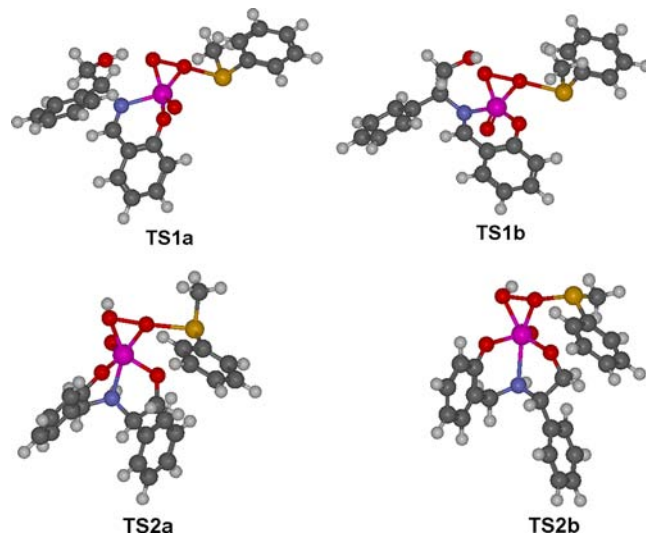
Several of the most stable isomeric forms found for the imino alcohol peroxido complex of 20 were also calculated for the corresponding amino alcohol peroxido species of 21 (Scheme 8 and Figure 2TS in the Supporting Information). As a result of

Scheme 8. Possible Isomeric Peroxido Species for the Model Compound 21



the geometry optimization of some hexacoordinated isomers (e.g., 21aa), the ligated water molecules were liberated from the coordination sphere of the metal, and the coordination number of vanadium in the resulting structures is 5. The calculations showed that the most stable isomer of 21 is the pentacoordinated hydroperoxido complex 21aa, a species of different nature compared with 20fa. Thus, complexes of the 20fa and 21aa types are the active catalytic species in sulfoxidation with the V^{IV} imino alcohol and amino alcohol systems, respectively.

Second, the mechanism of the thioanisole sulfoxidation was investigated, with the most stable isomers of 20 and 21 (i.e., 20fa and 21aa) taken as catalysts. The Sharpless-type mechanism is usually the one operating for the oxygen-transfer reactions (epoxidation and sulfoxidation) with hydrogen peroxide catalyzed by transition-metal complexes.⁵⁶ In this mechanism, sulfoxidation is considered as a concerted one-step process including the direct attack of the peroxido (or hydroperoxido) ligand of a catalyst by thioether. The transition states of the Sharpless mechanism were found for sulfoxidation of thioanisole with both 20fa and 21aa complexes (TS1a–TS1d and TS2a–TS2d, correspondingly, in Figure 9 and also 3TS in the Supporting Information). The geometry optimiza-

Figure 9. Most stable transition states leading to (*R*)-sulfoxides (TS1a and TS2a) and (*S*)-sulfoxides (TS1b and TS2b).

tion of TS1a–TS1d resulted in liberation of the coordinated water molecule from the coordination sphere of the metal, and the coordination number of vanadium in these transition states is either 5 or 6. TS1a, TS1c, TS2a, and TS2c lead to formation of the *R* enantiomer of sulfoxide, while other TSs afford the *S* enantiomer. The calculations showed the following: (i) The imino alcohol vanadium complexes, V(AOSB), are more efficient catalysts in this process than the amino alcohol vanadium species, V(AORSB); the lowest activation barriers for 20fa and 21aa are 99.2 and 121.3 kJ/mol, respectively (in terms of ΔG_s^\ddagger ; Table 9). (ii) The different nature of the active catalytic

Table 9. Gibbs Free Energies of Activation in CH₂Cl₂ Solution (in kJ/mol) for Sulfoxidation of Thioanisole Catalyzed by 20fa (TS1a–d, Corresponding to a Schiff Base Ligand) and 21aa (TS2a–d, Corresponding to a Reduced Schiff Base Ligand)

transition state	stereo configuration of the resulting sulfoxide	ΔG_s^\ddagger
TS1a	<i>R</i>	99.2
TS1b	<i>S</i>	100.4
TS1c	<i>R</i>	107.9
TS1d	<i>S</i>	109.6
TS2a	<i>R</i>	125.9
TS2b	<i>S</i>	121.3
TS2c	<i>R</i>	145.6
TS2d	<i>S</i>	124.7

species, 20fa (for the vanadium Schiff base ligand) and 21aa (for the vanadium-reduced Schiff base ligand), can explain the marked discrepancy of catalytic activities between the V(AOSB) and V(AORSB) compounds. (iii) The calculated activation energies for sulfoxidation are somewhat lower than the activation energies found previously for the olefin epoxidation reaction with related salan-based vanadium catalysts (134.3 kJ/mol).^{56d}

The calculations also showed that sulfoxidation should have very low stereoselectivity (or not at all) with both imino and amino alcohol catalysts despite the different nature of the active catalytic species 20fa and 21aa. The difference of the activation energies for the reaction channels leading to (*R*)- or (*S*)-sulfoxide is less than 5 kJ/mol for both catalysts 20fa and 21aa. Such a low stereoselectivity in both cases is because both catalysts 20fa and 21aa are coordinatively unsaturated and, hence, flexible species with a reduced level of steric hindrance. The significant enantiomeric excess obtained with the V(AOSB) compounds contradict, in part, this prediction, which means that other parameters must be factored into the calculation of the activation energies, namely, potential through-space electrostatic and aryl–aryl interactions. For the most part, the product stereoconfiguration prediction is consistent with the experimental results where, for instance, *S* catalysts yield (*S*)-sulfoxides, with the exception of compound 10, which has a *R* configuration but gave (*S*)-sulfoxide, albeit in very low yields. The product stereoconfiguration yield is also consistent with literature reports.^{30a}

CONCLUSIONS

Several chiral amino alcohol-derived V^{IV}O compounds were prepared, characterized, and employed as catalysts in the asymmetric sulfoxidation of thioanisole. The molecular structures of two of the reduced Schiff base amino alcohols (4 and 8) were determined, confirming the successful synthesis

of the AORSB compounds. Except in two cases, all V^{IV}O compounds were consistent with a dimeric [ML]₂ formulation, as was confirmed for 13.

The molecular structure of the V^{IV}O(AOSB) compound 13 was obtained by single-crystal X-ray diffraction, and to our knowledge, it constitutes the first example of a chiral V^{IV}O compound of this class. The structure is notable for its dinuclear syn-orthogonal V^{IV}O cores, which are 3.053(9) Å apart. Strong antiferromagnetic interactions are associated with edge-sharing orthogonal square-pyramidal V^{IV}O cores, and 13 is such a case, as evidenced by the extremely weak and unresolved EPR spectrum in solution. It is possible that the other EPR-silent V^{IV}O(AOSB) and V^{IV}O(AORSB) compounds adopt similar structures, given that EPR spectra were only obtained if strongly coordinating solvents such as DMF were used.

Spectroscopic studies were carried out despite the tendency of the V^{IV}O compounds to oxidize quickly in solution. The V^{IV}O(AOSB) compounds showed a higher resistance toward oxidation to V^V than the V^{IV}O(AORSB) compounds. This behavior is similar to what was observed with V^{IV}O-salen and -salan compounds studied previously by our group, where the presence of coordinating imine moieties stabilizes vanadium in its 4+ oxidation state.^{9a} CD studies show that these V^V species and the respective V^{IV} precursors exhibit optical activity associated with the charge-transfer and d–d transitions. Spectroscopic studies also indicate that phenolate-bound V^VO³⁺ species are formed after oxidation; however, the lower than expected intensity of the V–O_{phenolate} LMCT bands indicated that V^VO₂⁺ species are also present. EPR spectra were measured with the V^{IV}O(AORSB) compounds, and the obtained hyperfine coupling constants are consistent with *fac* conformations in solution, reflecting the flexibility of the AORSB ligands. In contrast, the studied V^{IV}O(AOSB) gave very weak or no EPR signals, which is indicative of spin–spin coupling between V^{IV}O cores with significant antiferromagnetic character. The theoretical DFT calculations together with the experimental EPR data allowed the establishment of the composition and structural features of the V^{IV}O(AOSB) and V^{IV}O(AORSB) species formed in solution.

⁵¹V NMR studies were carried out with representative V^{IV}O(AOSB) and V^{IV}O(AORSB) compounds with the intent of observing the intervenient V^V species generated in both cases. The measurements were successful with V^{IV}O(AOSB) compound 17, in which V^VO³⁺, V^VO₂⁺, and monoperoxido- and dioxovanadium species were assigned also with the aid of computational predictions.

Catalytic studies showed a distinct behavior between the V(AOSB) and V(AORSB) systems, with V(AOSB) being significantly more active and enantioselective. The main contributing factor for this marked difference is the existence of the C=N double bond, which transmits some rigidity to the systems. Phenolate moiety substituents also influence the enantioselectivity but to a much lower extent. Both observations above are in contrast with our initial expectations and also contrast with what was observed with the V-salen and -salan compounds, where the existence of a C–N single bond proved beneficial and the phenolate substituents exerted a significant influence on the enantioselectivity and catalyst activity.^{9a} Thus, although the good stability of the V(AORSB) systems may be a promising factor featuring their use as catalysts in heterogenized systems, the very low enantioselectivities obtained are disappointing.

The mechanistic DFT study allowed (i) determination of the active catalytic species for thioanisole sulfoxidation, which are of distinct nature, i.e., vanadium peroxo complex **20fa** and vanadium hydroperoxo species **21aa** for the V(AOSB) and V(AORSB) systems, respectively, and (ii) an explanation of the experimentally observed and theoretically confirmed higher catalytic activity of the V(AOSB) systems compared to the V(AORSB) ones. However, an adequate explanation for the marked differences in the enantioselectivity is still not possible with current models because other factors, such as through-space electrostatic and aryl–aryl interactions, must be taken into account.

■ ASSOCIATED CONTENT

■ Supporting Information

Listings of EPR hyperfine coupling constant estimates and plausible binding modes, isotropic visible and CD spectra, crystal packing figures, ^{51}V NMR spectra, and details of computational calculations. This material is available free of charge via the Internet at <http://pubs.acs.org>.

■ AUTHOR INFORMATION

Corresponding Author

*E-mail: (P.A.), joao.pessoa@ist.utl.pt (J.C.P.).

Notes

The authors declare no competing financial interest.

■ ACKNOWLEDGMENTS

The authors thank the Portuguese NMR Network (IST-UTL Center), POCI 2010, FEDER, Fundação para a Ciência e Tecnologia (Grants SFRH/BD/40279/2007, SFRH/BPD/79778/2011, and SFRH/BPD/73941/2010), PTDC/QUI-QUI/119561/2010, and PEst-OE/QUI/UI0100/2011 for financial support and the Spanish–Portuguese Bilateral Programme (Acção Integrada E-56/05 and Acción Integrada HP2004-00). S.B. would like to thank Prof. M. Teresa Duarte for valuable discussions on X-ray crystallography. M.L.K. is grateful to the FCT and IST for a research contract within the Ciência 2007 scientific programme.

■ REFERENCES

- Bolm, C.; Bienewald, F. *Angew. Chem., Int. Ed. Engl.* **1995**, *34*, 2640–2642.
- Nakajima, K.; Kojima, K.; Kojima, M.; Fujita, J. *Bull. Chem. Soc. Jpn.* **1990**, *63*, 2620–2630.
- Vetter, A. H.; Berkessel, A. *Tetrahedron Lett.* **1998**, *39*, 1741–1744.
- Jeong, Y.; Choi, S.; Hwang, Y. D.; Ahn, K. *Tetrahedron Lett.* **2004**, *45*, 9249–9252.
- Zeng, Q.; Wang, H.; Wang, T.; Cai, Y.; Weng, W.; Zhao, Y. *Adv. Synth. Catal.* **2005**, *347*, 1933–1936.
- Drago, C.; Caggiano, L.; Jackson, R. F. W. *Angew. Chem.* **2005**, *117*, 7387–7389.
- Cucciolo, M. E.; Del Litto, R.; Roviello, G.; Ruff, F. *J. Mol. Catal. A: Chem.* **2005**, *236*, 176–181.
- Liu, H.; Wang, H.; Wang, Y.; Wang, Y.; Sun, H.; Sun, L. *Catal. Commun.* **2009**, *11*, 294–297.
- (a) Adão, P.; Costa Pessoa, J.; Henriques, R. T.; Kuznetsov, M. L.; Aveçilla, F.; Maurya, M. R.; Kumar, U.; Correia, I. *Inorg. Chem.* **2009**, *48*, 3542–3561. (b) Adão, P.; Maurya, M. R.; Kumar, U.; Aveçilla, F.; Henriques, R. T.; Kuznetsov, M. L.; Costa Pessoa, J.; Correia, I. *Pure Appl. Chem.* **2009**, *81*, 1279–1296. (c) Adão, P.; Aveçilla, F.; Bonchio, M.; Carraro, M.; Costa Pessoa, J.; Correia, I. *Eur. J. Inorg. Chem.* **2010**, 5568–5578.
- (10) Rockenbauer, A.; Korecz, L. *Appl. Magn. Reson.* **1996**, *10*, 29–43.
- (11) (a) Sheldrick, G. M. *SADABS, Program for Empirical Absorption Correction*; University of Göttingen: Göttingen, Germany, 1996. (b) Flack, H. D.; Bernardinelli, G. *Acta Crystallogr., Sect. A* **1999**, *A55*, 908–915. (c) Flack, H. D.; Bernardinelli, G. *J. Appl. Crystallogr.* **2000**, *33*, 1143–1148.
- (12) Burla, M. C.; Caliandro, R.; Camalli, M.; Carrozzini, B.; Cascarano, G. L.; De Caro, L.; Giacovazzo, C.; Polidori, G.; Spagna, R. *J. Appl. Crystallogr.* **2005**, *38*, 381.
- (13) Sheldrick, G. M. *Acta Crystallogr.* **1990**, *A46*, 467.
- (14) Farrugia, L. J. *J. Appl. Crystallogr.* **1999**, *32*, 837.
- (15) (a) Sheldrick, G. M. *SHELXL-97—Programs for Crystal Structure Analysis*, release 97-2; University of Göttingen: Göttingen, Germany, 1998. (b) Sheldrick, G. M. *Acta Crystallogr.* **2008**, *A64*, 122.
- (16) Farrugia, L. J. *J. Appl. Crystallogr.* **1997**, *30*, 565.
- (17) (a) Becke, A. D. *J. Chem. Phys.* **1993**, *98*, 5648. (b) Lee, C.; Yang, W.; Parr, R. G. *Phys. Rev.* **1988**, *B37*, 785.
- (18) Frisch, M. J.; Trucks, G. W.; Schlegel, H. B.; Scuseria, G. E.; Robb, M. A.; Cheeseman, J. R.; Montgomery, J. A., Jr.; Vreven, T.; Kudin, K. N.; Burant, J. C.; Millam, J. M.; Iyengar, S. S.; Tomasi, J.; Barone, V.; Mennucci, B.; Cossi, M.; Scalmani, G.; Rega, N.; Petersson, G. A.; Nakatsuji, H.; Hada, M.; Ehara, M.; Toyota, K.; Fukuda, R.; Hasegawa, J.; Ishida, M.; Nakajima, T.; Honda, Y.; Kitao, O.; Nakai, H.; Klene, M.; Li, X.; Knox, J. E.; Hratchian, H. P.; Cross, J. B.; Adamo, C.; Jaramillo, J.; Gomperts, R.; Stratmann, R. E.; Yazyev, O.; Austin, A. J.; Cammi, R.; Pomelli, C.; Ochterski, J. W.; Ayala, P. Y.; Morokuma, K.; Voth, G. A.; Salvador, P.; Dannenberg, J. J.; Zakrzewski, V. G.; Dapprich, S.; Daniels, A. D.; Strain, M. C.; Farkas, O.; Malick, D. K.; Rabuck, A. D.; Raghavachari, K.; Foresman, J. B.; Ortiz, J. V.; Cui, Q.; Baboul, A. G.; Clifford, S.; Cioslowski, J.; Stefanov, B. B.; Liu, G.; Liashenko, A.; Piskorz, P.; Komaromi, I.; Martin, R. L.; Fox, D. J.; Keith, T.; Al-Laham, M. A.; Peng, C. Y.; Nanayakkara, A.; Challacombe, M.; Gill, P. M. W.; Johnson, B.; Chen, W.; Wong, M. W.; Gonzalez, C.; Pople, J. A. *Gaussian 03*, revision C.02; Gaussian, Inc.: Wallingford, CT, 2004.
- (19) Dolg, M.; Wedig, U.; Stoll, H.; Preuss, H. *J. Chem. Phys.* **1987**, *86*, 866–872.
- (20) Tomasi, J.; Persico, M. *Chem. Rev.* **1994**, *94*, 2027–2094.
- (21) Barone, V.; Cossi, M. *J. Phys. Chem. A* **1998**, *102*, 1995–2001.
- (22) Wertz, D. H. *J. Am. Chem. Soc.* **1980**, *102*, 5316–5322.
- (23) Cooper, J.; Ziegler, T. *Inorg. Chem.* **2002**, *41*, 6614–6622.
- (24) (a) Ditchfield, R. *Mol. Phys.* **1974**, *27*, 789–807. (b) Wolinski, K.; Hinton, J. F.; Pulay, P. *J. Am. Chem. Soc.* **1990**, *112*, 8251–8260.
- (25) Maurya, M. R.; Arya, A.; Kumar, A.; Kuznetsov, M. L.; Aveçilla, F.; Costa Pessoa, J. *Inorg. Chem.* **2010**, *49*, 6586–6600.
- (26) Gorelsky, S.; Micera, G.; Garribba, E. *Chem.—Eur. J.* **2010**, *16*, 8167–8180.
- (27) Carrano, C. J.; Nunn, C. M.; Quan, R.; Bonadies, J. A.; Pecoraro, V. L. *Inorg. Chem.* **1990**, *29*, 944–951.
- (28) Duan, Z.; Schmidt, M.; Young, V. G., Jr.; Xie, X.; McCarley, R. E.; Verkade, J. G. *J. Am. Chem. Soc.* **1996**, *118*, 5302–5303 and references therein.
- (29) (a) Plass, W. *Angew. Chem., Int. Ed.* **1996**, *35*, 627–631. (b) Ceccato, A. S.; Neves, A.; de Brito, M. A.; Drechsel, S. M.; Mangrich, A. S.; Werner, R.; Haase, W.; Bortoluzzi, A. J. *J. Chem. Soc., Dalton Trans.* **2000**, 1573–1577. (c) Tsaramyrsi, M.; Kaliva, M.; Salifoglou, A.; Raptopoulou, C. P.; Terzis, A.; Tangoulis, V.; Giapintzakis, J. *Inorg. Chem.* **2001**, *40*, 5772–5779. (d) Garribba, E.; Micera, G.; Lodyga-Chruscinska, E.; Sanna, D. *Eur. J. Inorg. Chem.* **2006**, 2690–2700.
- (30) (a) Bryliakov, K. P.; Karpyshev, N. N.; Fominsky, S. A.; Tolstikov, A. G.; Talsi, E. P. *J. Mol. Catal. A: Chem.* **2001**, *171*, 73–80. (b) Conte, V.; Furia, F. D.; More, S. *Inorg. Chim. Acta* **1998**, *272*, 62–67.
- (31) (a) Costa Pessoa, J.; Cavaco, I.; Correia, I.; Tomaz, I.; Duarte, M. T.; Matias, P. M. *J. Inorg. Biochem.* **2000**, *80*, 35–39. (b) Costa Pessoa, J.; Calhorda, M. J.; Cavaco, I.; Correia, I.; Duarte, M. T.; Felix,

V.; Henriques, R. T.; Piedade, M. F. M.; Tomaz, I. *J. Chem. Soc., Dalton Trans.* **2002**, 4407–4415.

(32) (a) Cashin, B.; Cunningham, D.; Daly, P.; McArdle, P.; Munroe, M.; Chonchubhair, N. N. *Inorg. Chem.* **2002**, *41*, 773–782. (b) Ebel, M.; Rehder, D. *Inorg. Chem.* **2006**, *45*, 7083–7090.

(33) (a) Correia, I.; Costa Pessoa, J.; Duarte, M. T.; Henriques, R. T.; Piedade, M. F. M.; Veiros, L. F.; Jakusch, T.; Kiss, T.; Dörnyei, Á.; Castro, M. M. C. A.; Geraldés, C. F. G. C.; Avecilla, F. *Chem.—Eur. J.* **2004**, *10*, 2301–2317. (b) Cavaco, I.; Costa Pessoa, J.; Duarte, M. T.; Henriques, R. T.; Matias, P. M.; Gillard, R. D. *J. Chem. Soc., Dalton Trans.* **1996**, 1989–1996.

(34) Rao, S. N.; Mishra, D. D.; Maurya, R. C.; Rao, N. N. *Polyhedron* **1997**, *16*, 1825–1829.

(35) Li, X.; Lah, M. S.; Pecoraro, V. L. *Inorg. Chem.* **1988**, *27*, 4657–4664.

(36) Carrano, C. J.; Nunn, C. M.; Quan, R.; Bonadies, J. A.; Pecoraro, V. L. *Inorg. Chem.* **1990**, *29*, 944–951.

(37) (a) Wüthrich, K. *Helv. Chim. Acta* **1965**, *48*, 1012–1017. (b) Chasteen, N. D. In *Biological Magnetic Resonance*; Berliner, L. J., Reuben, J., Eds.; Plenum Press: New York, 1981; Vol. 3, pp 53–119.

(38) Smith, T. S., II; LoBrutto, R.; Pecoraro, V. L. *Coord. Chem. Rev.* **2002**, *228*, 1–18.

(39) (a) Cornman, C. R.; Geiser-Bush, C. M.; Rowley, S. P.; Boyle, P. D. *Inorg. Chem.* **1997**, *36*, 6401–6408. (b) Micera, G.; Garribba, E. *Eur. J. Inorg. Chem.* **2011**, 3768–3780.

(40) Addison, A. W.; Rao, T. N.; Reedijk, J.; van Rijn, J.; Verschoor, G. C. *J. Chem. Soc., Dalton Trans.* **1984**, 1349–1356.

(41) Micera, G.; Garribba, E. *Eur. J. Inorg. Chem.* **2010**, 4697–4710.

(42) Ballhausen, C. J.; Gray, H. B. *Inorg. Chem.* **1962**, *1*, 111–122.

(43) Vilas Boas, L.; Costa Pessoa, J. Vanadium. In *Comprehensive Coordination Chemistry*; Wilkinson, G., Gillard, R. D., McCleverty, J. A., Eds.; Oxford University Press: New York, 1987; Vol. 3, pp 453–583.

(44) (a) Colpas, G. J.; Hamstra, B. J.; Kampf, J. W.; Pecoraro, V. L. *Inorg. Chem.* **1994**, *33*, 4669–4675. (b) Sharma, N.; Sood, A. K.; Bhatt, S. S.; Chaudhry, S. C. *Polyhedron* **1997**, *16*, 4055–4060. (c) Neves, A.; Ceccatto, A. S.; Erasmus-Buhr, C.; Gehring, S.; Haase, W.; Paulus, H.; Nascimento, O. R.; Batistae, A. A. *J. Chem. Soc., Chem. Commun.* **1993**, 1782–1784.

(45) Costa Pessoa, J.; Cavaco, I.; Correia, I.; Duarte, M. T.; Gillard, R. D.; Henriques, R. T.; Higes, F. J.; Madeira, C.; Tomaz, I. *Inorg. Chim. Acta* **1999**, *293*, 1–11.

(46) (a) Asgedom, G.; Sreedhara, A.; Kivikoski, J.; Valkonen, J.; Kolehmainen, E.; Rao, C. P. *Inorg. Chem.* **1996**, *35*, 5674–5683. (b) Maurya, M. R.; Agarwal, S.; Bader, C.; Ebelband, M.; Rehder, D. *Dalton Trans.* **2005**, 537–544.

(47) (a) Wolff, F.; Lorber, C.; Choukroun, R.; Donnadiou, B. *Inorg. Chem.* **2003**, *42*, 7839–7845. (b) Barroso, S.; Adão, P.; Madeira, F.; Teresa Duarte, M.; Costa Pessoa, J.; Martins, A. M. *Inorg. Chem.* **2010**, *49*, 7452–7463.

(48) (a) Rehder, D.; Weidemann, C.; Duch, A.; Pribsch, W. *Inorg. Chem.* **1988**, *27*, 584–587. (b) Pribsch, W.; Rehder, D. *Inorg. Chem.* **1990**, *29*, 3013–3019.

(49) Avecilla, F.; Adão, P.; Correia, I.; Costa Pessoa, J. *Pure Appl. Chem.* **2009**, *81*, 1297–1311.

(50) Pettersson, L.; Andersson, I.; Gorzsas, A. *Coord. Chem. Rev.* **2003**, *237*, 77–87.

(51) Cornman, C. R.; Colpas, G. J.; Hoeschele, J. D.; Kampf, J.; Pecoraro, V. L. *J. Am. Chem. Soc.* **1992**, *114*, 9925–9933.

(52) Roy, N.; Sproules, S.; Bothe, E.; Weyhermüller, T.; Wieghardt, K. *Eur. J. Inorg. Chem.* **2009**, 2655–2663.

(53) (a) Blum, S. A.; Bergman, R. G.; Ellman, J. A. *J. Org. Chem.* **2003**, *68*, 150–155. (b) Conte, V.; DiFuria, F.; Moro, S. *J. Mol. Catal. A: Chem.* **1997**, *117*, 139–149.

(54) (a) Pozarnsky, G. A.; McCormick, A. V. *J. Mater. Chem.* **1994**, *4*, 1749–1753. (b) Lu, X. *Electrochim. Acta* **2001**, *46*, 4281–4287.

(55) Zeng, Q.; Wang, H.; Wang, T.; Cai, Y.; Weng, W.; Zhao, Y. *Adv. Synth. Catal.* **2005**, *347*, 1933–1936.

(56) (a) Seenivasaperumal, M.; Federsel, H.-J.; Szabó, K. J. *Adv. Synth. Catal.* **2009**, *351*, 903. (b) Schneider, C. J.; Penner-Hahn, J. E.; Pecoraro, V. L. *J. Am. Chem. Soc.* **2008**, *130*, 2712. (c) Zampella, G.; Fantucci, P.; Pecoraro, V. L.; Gioia, L. D. *J. Am. Chem. Soc.* **2005**, *127*, 953. (d) Kuznetsov, M. L.; Pessoa, J. C. *Dalton Trans.* **2009**, 5460. (e) Yudanov, I. V. *J. Struct. Chem.* **2007**, *48*, S111. (f) Conte, V.; Coletti, A.; Floris, B.; Licini, G.; Zonta, C. *Coord. Chem. Rev.* **2011**, *255*, 2165.